Università degli Studi di Padova

Department of Information Engineering

Master's in ICT and Multimedia Engineering

(Photonics Curriculum)

MASTER'S THESIS

Investigating polarization conversion in a planar array of High Refractive Index all-dielectric nanospheres using the Coupled Electric and Magnetic Dipole formulation

THESIS SUPERVISOR
Prof. Marco Santagiustina

INTERNSHIP SUPERVISOR
Prof. José Antonio Sanchez-Gil

STUDENT
Ruhinda Kabonire

ASSISTANT SUPERVISOR
Dr. Diego Romero Abujetas
Prof. Domenico De Ceglia

Padova, 3rd October 2022

ACADEMIC YEAR 2021/22

CSIC
Consejo Superior de Investigaciones Científicas

Ruhinda Kabonire	Marco Santagiustina

“There’s Plenty of Room at the Bottom”

RICHARD FEYNMAN

Table of contents:

List of acronyms:

1	BIC	Bound state In the Continuum
2	HRI	High Refractive Index
3	CEMD	Coupled Electric and Magnetic Dipole
4	TE	Transverse Electric
5	TM	Transverse Magnetic
6	NS	Nano Sphere
7	MS	Meta Surface
8	ND	Nano Disk
9	NR	Nano Resonator
10	ED	Electric Dipole
11	MD	Magnetic Dipole
12	EQ	Electric Quadrupole
13	MQ	Magnetic Quadrupole
14	LP	Linearly Polarised
15	RHCP	Right Handed Circularly Polarised
16	LHCP	Left Handed Circularly Polarised
17	1D	One - dimensional
18	2D	Two - dimensional
19	Si	Silicon

List of figures:

INTRODUCTION

Electromagnetic optics is a vector theory consisting of mutually coupled electric and magnetic fields, which vary in space and time and propagate as an electromagnetic field wave. The propagation direction, defined by the wave vector ***k*** is usually orthogonal to the electric and magnetic field components, hence the name transverse electric and magnetic (TEM) field wave, as shown below.

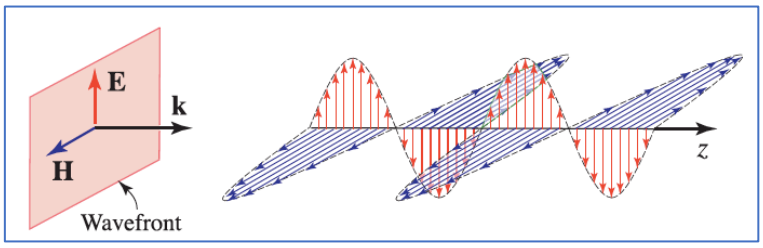

Figure 1: Transverse electromagnetic field

Light-matter interactions exist at the sub-atomic scale, with the energy of the said range of frequency radiation matching matter's electronic and vibrational transition states. Through this, we can not only attain the properties of matter, but also have the ability to manipulate its quantum states.

Electromagnetic radiation can present itself with particles of light known as photons, but also with wave-like properties, as observed in various quantum-mechanical experiments. Wave-like behaviour is more common at the longer wavelength side of the electromagnetic spectrum, while particle-like behaviour, with the higher-frequencies. The figure below brings a clearer picture of the layout of the electromagnetic spectrum, which can be defined as an allowed range of frequencies of oscillation, demarcated by several bands ranging from gamma rays to radio waves.

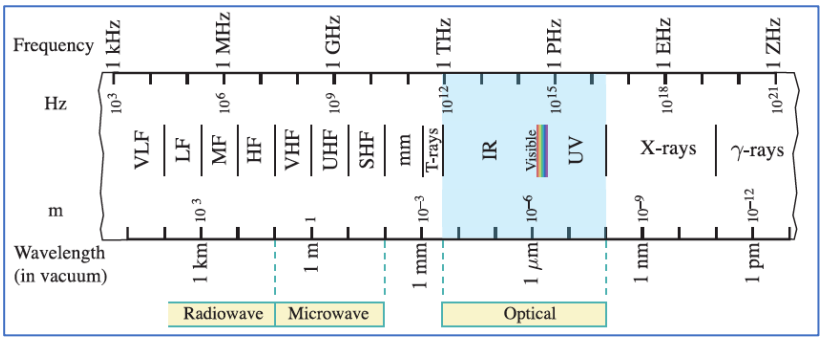

Figure 2: The electromagnetic spectrum (1).

This thesis considers the interaction of plane waves at wavelengths within the range of $0.353 - 1\ \mu m$ (generally referred to as optical frequencies), incident on a planar array of periodically arranged High Refractive Index (HRI) nanospheres (Silicon), oriented with one particle per unit cell, in the specular diffraction regime.

Analysis of the said patterns portraying the refractive and reflective properties of the metasurface is easily expressed by a dimensionless frequency expression $\frac{ka}{2\pi}$, where k stands for the wave number of the impinging wave, and a stands for the lattice periodicity of the metasurface.

A brief introduction to the theory related to the subject is presented below, from the basic principles of electromagnetic systems, to the deep details explaining the behaviour of the system at resonant frequencies.

Through this thesis, parallels are drawn between the use of all-dielectric nanoparticles, and the plasmonic counterparts studied through literature, highlighting the advantages of the current method, the most important of them being the functional efficiency.

We also define and characterise the photonic Bound states In the Continuum (BICs) present in such metasurface structures.

LITERATURE REVIEW

Maxwell's Equations

In order to sufficiently describe optical radiation in nano-optics, the field theory based on Maxwell's equations is considered.

James Clerk Maxwell shaped electromagnetism, unifying the laws of electric and magnetic fields. He initially composed 20 simultaneous equations with 20 different unknown variables, which could not account for any fields which were constant in space and time. However, through the work (majorly) of Oliver Heaviside, and several other notable physicists of the 19th century, the equations were condensed into the 4 commonly used expressions.

They can now either be expressed in their integral or differential form, by applying Stokes' theorem, the divergence theorem and/ or the continuity equation.

i). Faraday's law

Faraday's law of induction shows the relationship between the time-varying magnetic flux and a spatially varying electric field, through the curl operator.

$$\nabla \times \boldsymbol{E}(\boldsymbol{r}, t) = \frac{-\partial \boldsymbol{B}(\boldsymbol{r}, t)}{\partial t}$$

$\boldsymbol{E}$ is the electric field, $[V/m]$, while $\boldsymbol{B}$ is the induction field, $[T]$

ii). Ampere's law

Ampere's law expresses the interconnection between the magnetomotive force and the current flowing through a surface. Free charge current and the displacement current contributions ensure charge conservation in the system.

$$\nabla \times \boldsymbol{H}(\boldsymbol{r}, t) = \frac{\partial \boldsymbol{D}(\boldsymbol{r}, t)}{\partial t} + \boldsymbol{J}(\boldsymbol{r}, t)$$

$\boldsymbol{H}$ is the magnetic field $[A/m]$, $\frac{\partial \boldsymbol{D}(\boldsymbol{r},t)}{\partial t}$ represents the displacement current, while $\boldsymbol{J}$ represents the current density $[A/m^2]$.

iii). Gauss' law for electricity

It represents the relationship between the displacement field and free charge density. In its integral form, Gauss's law tells us that the net electric flux through any closed surface is zero

unless the volume bounded by that surface contains a net charge. In its differential form on the other hand, it shows equivalence to Coulomb's law.

$$\nabla . \boldsymbol{D}(\boldsymbol{r}, t) = \rho(\boldsymbol{r}, t)$$

$\boldsymbol{D}$ is the electric flux density (electric displacement) $[C/m^2]$, ρ represents the charge density$[C/m^3]$.

iv). Gauss' law for magnetism

Gauss' law expresses the lack in nature of magnetic sources or sinks, or rather commonly known as *monopoles*.

$$\nabla \cdot \boldsymbol{B}(\boldsymbol{r}, t) = 0$$

B is the magnetic flux density (magnetic induction) $[T]$.

The 4 equations shown above are harmonised by the expressions we know as the **constitutive relations**, which are based on the properties of the material under consideration.

The material properties account for the cumulative electromagnetic response of a material averaged over many atoms, as long as the atoms are much smaller than the spatial variations of the electromagnetic fields involved.

i). Permittivity (ε) relates the electric field intensity to the displacement.

$$\boldsymbol{D}(\boldsymbol{r}, t) = \varepsilon \boldsymbol{E}(\boldsymbol{r}, t) \ = \varepsilon_0 \varepsilon_r \boldsymbol{E}(\boldsymbol{r}, t)$$

- ε_0 is the free space permittivity $(\sim 1/36\pi \times 10^{-9})$ $[F/m]$
- ε_r is the relative permittivity (dielectric constant) $= \frac{\varepsilon}{\varepsilon_0}$

ii). Permeability (μ) related the magnetic field intensity to the magnetic flux density.

$$\boldsymbol{B}(\boldsymbol{r}, t) = \mu \boldsymbol{H}(\boldsymbol{r}, t) = \mu_0 \mu_r \boldsymbol{H}(\boldsymbol{r}, t)$$

- μ_0 is the free space permeability $(4\pi \times 10^{-7})$ $[H/m]$
- μ_r is the relative permeability $= \frac{\mu}{\mu_0}$

iii). Electric conductivity (σ) relates the electric field intensity to the current density.

$$\boldsymbol{J}(\boldsymbol{r}, t) = \sigma \boldsymbol{E}(\boldsymbol{r}, t)$$

- σ is the electric conductivity $[S/m]$

By the material properties shown above, crucial aspects of the material properties considered are then obtained.

i). <u>Velocity of light in free space</u>

$$c_0 = \frac{1}{\sqrt{\mu_0 \varepsilon_0}} \qquad \sim 3 \times 10^8 \, [m/s]$$

ii). <u>Refractive index of a material</u>

$$n = \sqrt{\mu_r \varepsilon_r}$$

In the optical regime, the magnetic permeability μ for naturally occurring materials is always close to its free space value. This is due to the fact that the coupling of the magnetic field component of light to atoms is much weaker than that of the electric counterpart, a situation we refer to as a "one-handed" interaction (2).
This implies that $\mu_r = 1$, such that $n = \sqrt{\varepsilon_r}$.

iii). <u>Intrinsic impedance of the material</u>

$$\eta_0 = \sqrt{\frac{\mu_0}{\varepsilon_0}} \qquad \sim 120\pi \, [\Omega]$$

Usually, the electromagnetic properties of a material are discussed in terms of its macroscopic polarisation (average electric dipole moment per unit volume) **P** and magnetisation (average magnetic dipole moment per unit volume) **M** according to the following relations, which also stem from the constitutive relations.

$$\boldsymbol{D}(\boldsymbol{r}, t) = \varepsilon_0 \boldsymbol{E}(\boldsymbol{r}, t) + \boldsymbol{P}(\boldsymbol{r}, t), \qquad (\boldsymbol{P} = \varepsilon_0 \chi_e \boldsymbol{E})$$
$$\boldsymbol{B}(\boldsymbol{r}, t) = \mu_0 \boldsymbol{H}(\boldsymbol{r}, t) + \boldsymbol{M}(\boldsymbol{r}, t), \qquad (\boldsymbol{M} = \mu_0 \chi_m \boldsymbol{H})$$

We can conclude from the above expressions that the following relationships hold true;

$$\varepsilon_r = 1 + \chi_e, \qquad \mu_r = 1 + \chi_m$$

With χ_e and χ_m representing the electric field susceptibility (a measure of how easily the material can be polarised) and magnetic field magnetizability (a measure of how easily the material can be magnetised). From the explanation on the magnetic field interaction in the optical regime, the magnetic response $\chi_m \sim 0$.

It should also be noted that the polarisation and magnetisation densities expand to include the magnetoelectric cross polarisation terms, which are in turn responsible for polarisation conversion.

$$\boldsymbol{P}(\boldsymbol{r},t) = \varepsilon_0 \chi_e \boldsymbol{E}(\boldsymbol{r},t) + \chi_{em} \boldsymbol{H}(\boldsymbol{r},t)$$

$$\boldsymbol{M}(\boldsymbol{r},t) = \chi_m \boldsymbol{H}(\boldsymbol{r},t) + \frac{\chi_{me}}{\mu_0} \boldsymbol{H}(\boldsymbol{r},t)$$

By considering the polarisation and magnetisation mentioned above, a more comprehensive description of the material behaviour is attained.

i). Materials are classified as linear if their susceptibility is independent of the Electric field strength E, as the higher order terms of the susceptibility are irrelevant at low field intensities.

ii). It is considered to be homogeneous, if the response is independent of the position in the material at which it is characterised

iii). A material response is considered to be isotropic if the material permittivity (or permeability if considering another frequency regime) is independent of the direction of propagation of the radiation (it is a scalar rather than a tensor).

iv). We can say that a material is non-dispersive if the response is independent from space and time variations.

Polarisation

Polarisation is defined as the time-varying behaviour of the electric field intensity vector in space over a complete cycle. In the most general sense, the polarisation vector of a monochromatic wave presents a sinusoidal variation of any two orthogonal components of a complex amplitude vector for that given point, which is tangential to the plane in which the wavefront at the position is, tracing our an elliptically shaped pathway.

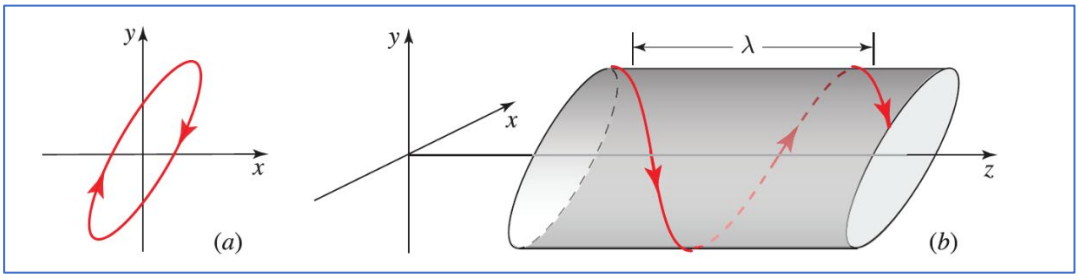

Figure 3: Schematic of an elliptically polarised wave with the wave vector in the z direction, wavelength λ.

However, in controlled cases (modification of amplitude and/ or phase), we can attain linear and circular polarisation of light from the general case of elliptically polarised light.

Polarisation of light that's travelling through different materials with differing material properties greatly depends on the boundary conditions. A TEM field can either have one of two orientations; transverse electric (TE), and transverse magnetic (TM) polarisation as shown in the figure below.

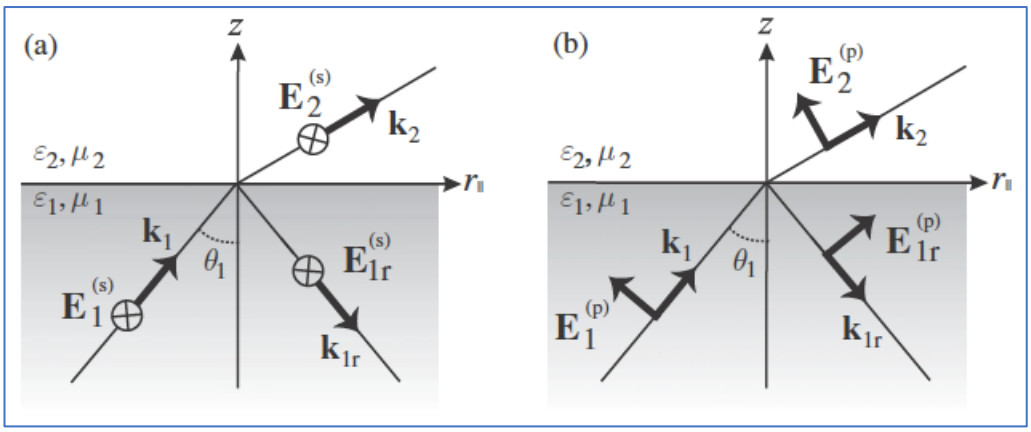

Figure 4: s-polarised light (a) and p-polarised light (b)

From the right-hand rule, we know that the magnetic field (not shown here) is mutually orthogonal to the electric field vector, the wave vector (given by $\boldsymbol{k} = k\hat{k}$) where $\hat{k}$ is a unit vector which lies along the plane of incidence (z, r_s in this case) and k is the wave number given by $k_0 n$.

In this case, using the cross on the $\boldsymbol{E}_1$ and $\boldsymbol{E}_2$ fields, we mean that their unit vectors point into the paper, then those of the magnetic fields point towards the media 1 and 2 interface, and tangential to the plane of incidence, as is the wave vector.

s-polarised light is derived from the German word "senkrecht", which means perpendicular. In this case, the electric field vector is perpendicular to the plane of incidence, while the wave vector and magnetic field vectors lie along the plane of incidence.

p-polarised light follows a similar explanation. The magnetic field vector is perpendicular to the plane of incidence. Through modern literature, several authors label TE waves as s-polarised, and TM waves as p polarised, but all of this depends greatly on the axial considerations made at the time of assessment.

In the most general sense, light is elliptically polarised. It can however be transformed to a circularly or linearly polarised wave by adjusting the amplitude and phase of the individual components. Considering the Cartesian 3 dimensional space with E_x and E_y as the electric field components in the x and y direction respectively for a wave whose propagation is along the z axis, by adopting the Jones vector formalism, or attaining the Stokes parameters, the state of polarisation can be altered at will.

i). Jones vectors

- Linear polarisation

For this polarisation at an angle θ, between the horizontal axis (for instance) and the electric field vector, the linear polarisation is given as shown below.

$$LP_\theta = \begin{bmatrix} \cos\theta \\ \sin\theta \end{bmatrix}$$

With this formalism, both the Jones vectors corresponding to horizontally and vertically polarised light can be obtained, with $\theta = 0°$ and $90°$ respectively.

$$LP_0 = \begin{bmatrix} 1 \\ 0 \end{bmatrix}, \qquad LP_{90} = \begin{bmatrix} 0 \\ 1 \end{bmatrix}$$

- Circular polarisation

By extension from the above, and by incorporating the use of Euler's relation to account for the 90° phase shift between the orthogonal components, the left-handed and right-handed circular polarisation expressions are given by

$$CP_{LH} = \frac{1}{\sqrt{2}}\begin{bmatrix} 1 \\ -j \end{bmatrix}, \qquad CP_{RH} = \frac{1}{\sqrt{2}}\begin{bmatrix} 1 \\ j \end{bmatrix}$$

It should also be noted that for circular polarisation, the amplitudes of the perpendicular components **have to be equal**.

ii). Stokes parameters

From the polarisation ellipse obtained from the Poincaré sphere, the Stokes' parameters can be obtained, as shown below.

$$I = |A_x|^2 + |A_y|^2$$

$$Q = |A_x|^2 - |A_y|^2$$

$$U = 2Re\{A_x^* A_y\}$$

$$V = 2Im\{A_x^* A_y\}$$

I is proportional to the intensity of the wave, while Q, U and V are related to the angle on the azimuthal axis (which defines the ellipse orientation), and the angle on the polar axis (which characterises the ellipticity considered within the Poincaré sphere).

Since $I^2 = Q^2 + U^2 + V^2$, only Q, U and V are independent variables, which can be used to completely define the state of polarisation of the incident light (1).

If in one case, linearly polarised light at 45° and 135° is considered, and on the other, left-handed and right-handed circularly polarised light, expressions for the U and V Stokes' parameters are expressed as shown.

$$U = |A_{45}|^2 - |A_{135}|^2$$
$$V = |A_R|^2 - |A_L|^2$$

Which brings the deduction that the V parameter contains information related to circularly polarised light, while the U parameter, for light oriented at 45° to the axes (in either direction).

To note: the state of polarisation of a normal mode is not changed when the wave is transmitted through the polarisation medium.

2.2.1 Polarisation conversion

In this modern age dominated by nano-photonics research, having the ability to fully control light is paramount, and is attainable by designs which are capable of $0 \rightarrow 2\pi$ phase modulation, and/ or amplitude modulation (3). Similar to the implementation in reflect and transmit arrays which were originally designed for use in the radio frequency spectrum, metasurface design utilises their asymmetric electric dipole resonances to allow $0 \rightarrow 2\pi$ phase control for the scattered cross-polarized light.

Unlike the plasmonic arrays, all-dielectric metasurfaces don't suffer Ohmic loss, and are capable of supporting both Electric Dipole (ED) and Magnetic dipole (MD) responses, due to the Mie resonances. However, at off-normal incidence, these resonators couple with each other at optical frequencies, due to their modest refractive indices (3).

Experimentation prior to this has been able to show that nearly perfect absorption, linear-to-circular polarisation conversion, and linear cross-polarization conversion can be integrated into one multifunctional metasurface. Furthermore, the multifunctional metasurface can maintain very high performance across a large range of incident angles (4).

Reflection and refraction in dielectric media

A reflected wave at an interface takes the opposite trajectory, so that it returns to the media from which it came, while a refracted wave, also otherwise known as the transmitted wave, progresses in a similar direction as the incident wave.

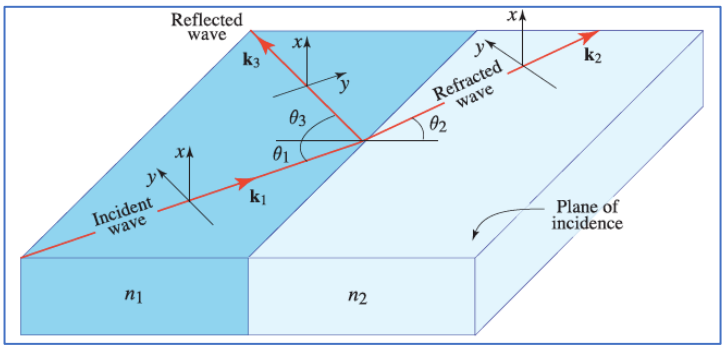

Figure 5: 3D schematic of light at an interface showing reflection and transmission (1)

The wave response to a boundary between the two materials with varying properties (refractive indices) as shown above can be broken into 4 case points. In general, if the index of the medium of incidence is less than the other ($n_1 < n_2$), we have what is known as **external reflection**, and for the reverse condition ($n_1 > n_2$), **internal reflection**.

When $n_1 < n_2$ for TE polarisation

The value of the reflection coefficient (r) is always real and negative due to the π phase shift, and its value gradually increases from $\frac{n_2-n_1}{n_2+n_1}$ at normal incidence to 1 at grazing incidence.

When $n_1 > n_2$ for TE polarisation

The value of "r" at normal incidence is given by $\frac{n_1-n_2}{n_1+n_2}$, but $r = 1$ is attained at the critical angle $\theta_c = \sin^{-1}\frac{n_2}{n_1}$ and beyond, a condition very commonly known as **total internal reflection (TIR)**.

When TIR is attained, an evanescent wave is created at the boundary of the interface of the materials.

When $n_1 < n_2$ for TM polarisation

The value of "r" is real and negative at normal incidence, equivalent to $\frac{n_1-n_2}{n_1+n_2}$, which then decreases until $r = 0$ (at the **Brewster angle**), denoted by the expression $\theta_B = \tan^{-1}\left(\frac{n_2}{n_1}\right)$. Beyond θ_B, there is a rapid growth in r, such that it grows to 1 at grazing incidence.

To note: Brewster's angle for a homogeneous isotropic non-magnetic media can be defined as the angle for which the Fresnel reflection coefficient for p-polarized light vanishes. One can obtain LP light from unpolarised light by impinging the material at the Brewster angle.

When $n_1 > n_2$ for TM polarisation

The value of "r" at normal incidence is $\frac{n_1 - n_2}{n_1 + n_2}$. It varnishes at θ_B, after which r grows negatively until unity magnitude at θ_c, and eventually TIR, which births an evanescent wave at the interface of materials 1 and 2.

From the reflection and transmission coefficients (r and t), the reflectance and transmittance (R and T), which represent the percentage of the incident wave's power is reflected and refracted respectively are obtained.

The expressions below hold true for the normal incidence case, but at a sub-atomic level, as the case of a metasurface, they hold if the medium of incidence is similar to that into which the transmission is expected.

$$R = |r|^2, \qquad T = \frac{n_2}{n_1}|t|^2$$

$$T = 1 - R$$

One key factor to note is the fact that most materials at optical frequencies have a relative permeability of 1, which only allows Brewster effects to be visible in p (TM) polarisation, which is the case for the material system considered for this thesis.

However, when consideration is extended to magneto-dielectrics, this value is not , which means that the Brewster effect can also be observed in TE polarisation (1).

Scattering of electromagnetic waves

Scattering of an incident electromagnetic field is greatly dependent on the relative size of the scatterers of the said radiation. Considering the spectrum shown below, which is representative of a nano sphere,

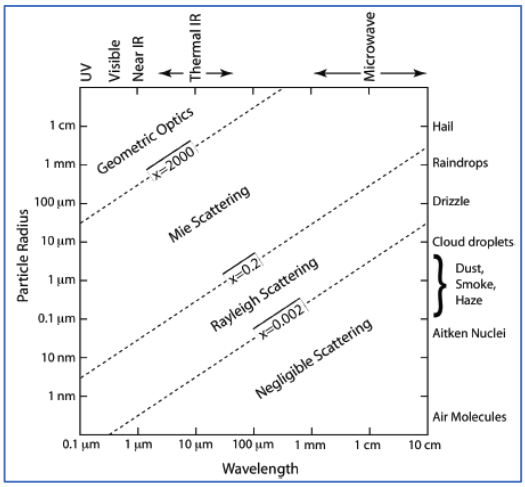

Figure 6: Scattering regimes for single spherical scatterers, based on relative particle size

If a particle has size dimension a, then the relative size of the particle used to ascertain the scattering regime is given as shown.

$$x = ka, \qquad x = \frac{2\pi}{\lambda} a$$

Where k is the wave number of the material, and a, the particle radius.

Unlike Rayleigh scattering whose radiation pattern is almost isotropic, the Mie scattering pattern is almost entirely unidirectional, depending on the size of the particle, and in the event that the particle size is larger than the wavelength of the incident light, the scattered power is proportional to the square of the particle diameter (1).

Figure 7: Rayleigh vs. Mie scattering radiation pattens

Metasurfaces

A metamaterial is an engineered 3D material, composed of "artificial atoms", known as the nanoscale scatterers, whose dimensions are much smaller than the operational wavelength of the system, and the goal of design is to enable them to yield qualities which are superior to those in conventional materials.

The essence of metamaterial design is to create materials whose parameters have a comfortable association with Maxwell's equations, giving the designer an upper hand in the control of electromagnetic waves, and one such application is having the ability to scatter light in a predefined fashion, ergo, obtaining novel material properties (2).

Since the resonant activity in metamaterials is greatly controlled by the geometry of its unit cell, in order to avoid diffraction effects, the periodicity of the scatterers must be much smaller than the wavelength under consideration. By this, we can see that the optical response of a metamaterial is the same as that of a piecewise homogeneous medium, having its electromagnetic properties relying mainly on the unit cell, rather than the periodic effects of the entire material.

There are subclasses under metamaterials, but the primary focus as it pertains to the discussion in this thesis is on metasurfaces, which are simply a 2D-version of a metamaterial.

Metasurfaces are usually created by assembling arrays of miniature, anisotropic light scatterers (resonators), but the condition is that both the **periodicity and size** of these resonators have to be **smaller** than the operational wavelength.

They are not only limited to periodic scatterers, since designs based on thin films also exist, although the former yield considerably greater flexibility, as much of the control of light interaction is based on the ability to manipulate the dimensions of the particles and lattice orientation.

This thesis' focus is on a metasurface composed of a periodic array of silicon nanospheres in air, forming a uniform square array as the plane of incidence, with one particle per unit cell, each of which is excited by a combination of both an impinging plane wave, and the scattered fields from the neighbouring particles.

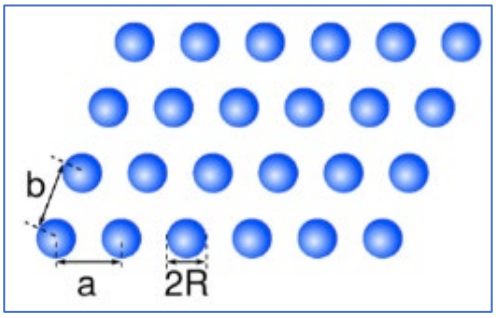

Figure 8: Layout of the silicon nanoparticles' array

Where

- Lattice constants: $a = b = 300\ nm$
- NP size (sphere radius): $R = {}^{a}/_{4}$

Some of the advantages of having the metasurface (MS) designed from all-dielectric HRI resonators include the fact that tailored light polarisation is achieved, along with specified light localisation. Additionally, the resonant optical modes enable nanoscale light manipulation, below the free-space diffraction limit (5).

Similar to plasmonic split-ring resonators or related geometries, high-permittivity dielectric nanoparticles provide a **strong magnetic response**, which is based on the excitation of the circular displacement currents inside the dielectric.

A metasurface of this nature also typically exhibits very low transmission at resonance, because, unlike the fictitious secondary sources of Huygens' principle, the fields scattered by these NRs are not forward-propagating (6).

All-dielectric meta-optics employs electric and magnetic Mie resonances of subwavelength particles with high refractive index for an optically induced magnetic response, thus underpinning a new approach to design and fabricate functional and practical meta-devices (6).

The design of artificial subwavelength meta-atoms that support a strong magnetic response, usually termed as optical magnetism exist, even with nonmagnetic metasurfaces (7).

Resonances

A resonance is a relatively large selective response of an object or system that vibrates in phase with an externally applied oscillatory force.

Considering a typical dielectric medium with complex susceptibility, its real part contributes to the frequencies near and below the resonant, while the imaginary part corresponds to those close to the resonant frequency. Knowledge of this enables the easy attainment of the information pertaining to the dispersion and absorption in a given material.

When specific consideration is given to a periodic array of nanoparticles, **multiple scattering** of light yields a structural resonance. The control of both the width of this resonance and its spectral location is governed by the size, distance of separation and quantity of the nano resonators in the array.

By this, an infinite array yields extremely narrow resonances for a certain ratio between the size and periodicity of the particles (8).

A very special example of a resonance in optics is the **Fano resonance**, which occurs when a discrete quantum state interferes with a continuous band of states, as witnessed in the absorption spectrum $\sigma(E)$, and this relationship is modelled by the famous Fano formula,

$$\sigma(E) = D^2 \frac{(q+\Omega)^2}{1+\Omega^2} \quad (9)$$

- E is the energy
- $q = \cot\delta$ is the Fano parameter
- δ is the phase shift of the continuum
- $\Omega = \frac{2(E-E_0)}{\Gamma}$ which gives information about the resonant position
- Γ and E_0 are the resonance width and energy respectively
- $D^2 = 4\sin^2\delta$

The resulting spectra below shows typical asymmetry with a sharp change between a dip and a peak.

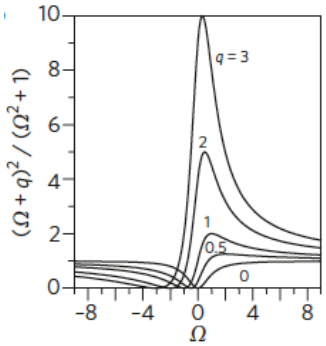

Figure 9: Typical asymmetrical shape associated to a Fano resonance (9).

When considering dielectric nanoparticles, particularly the interaction between the radiative and nonradiative modes, Fano resonances are linked to the interference relationship between multipole modes of the same type. Specifically important to note is the fact that magnetic-dipole resonances of individual dielectric particles play a crucial role in the appearance of the **Fano resonances** (6).

2.5.1 Mie resonances

According to the Mie theory, dielectric nanoparticles exhibit strong magnetic resonances in the visible spectrum. It also follows from the same theory that for a multipolar excitation of a subwavelength particle, the scattering efficiency is independent of the type of material, which gives dielectric MSs an edge over the plasmonic counterparts, since they have way less absorption losses at visible frequencies.

The electric and magnetic Mie resonances from subwavelength resonators substantially influence the scattering intensity and radiation pattern of the material, and due to the nanoscale localisation of the fields, nonlinear effects can be experienced in the material.

On the other hand, multimodal interference is a fuel and driving force to novel effects within metamaterials, such as the famous bounded states in the continuum. With scattered fields being composed of both electric and magnetic multipoles, the magnetic multipoles are the clincher of all-dielectric resonant meta-optics (10).

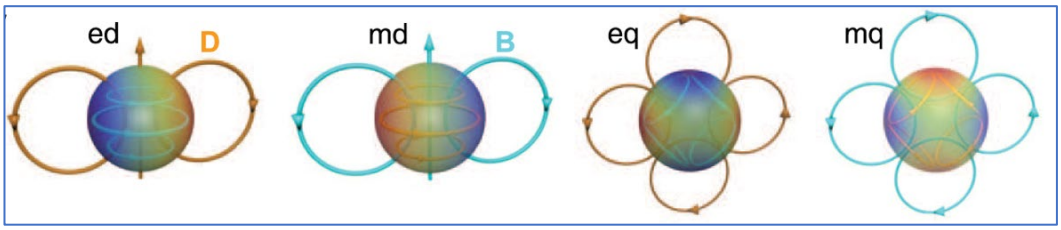

Figure 10: The field structure of the four major resonant modes in high-index dielectric particles (5).

Mie scattering is characterized by partial intensities and radiation patterns of dominant excited multipole modes, such as those shown in figure 9 above. The MD resonances of individual dielectric particles play a crucial role in the appearance of the Fano resonances. (10).

BICs

Bound states in the continuum (BICs) are waves which remain localized (with infinite lifetimes), while coexisting with a continuous spectrum of radiating waves, generally requiring the extension of at least one of the structure's dimensions to infinity (11).

Not only have they been identified in electromagnetic, but also acoustic, water and elastic waves. They were first proposed in quantum mechanics by Von Neumann and Wigner, whose chosen potential was highly oscillatory and could not be implemented in reality (12).

For an electromagnetic waves' system, there are two highly likely scenarios that could occur; a **confined wave**, whose energy/ frequency differs from that of the spectrum, thus hindering its transmission, or a **resonant wave**, whose energy matches that of the spectrum, so that it couples to the continuum of radiation and can escape to infinity.

The BIC adamantly defies this convention, because it not only lies inside the continuum, but also retains its confinement **without any radiation** (11).

The illustration in the figure below paints a picture of a typical open system carrying oscillatory energy, outlining the obvious characteristics of its constituents.

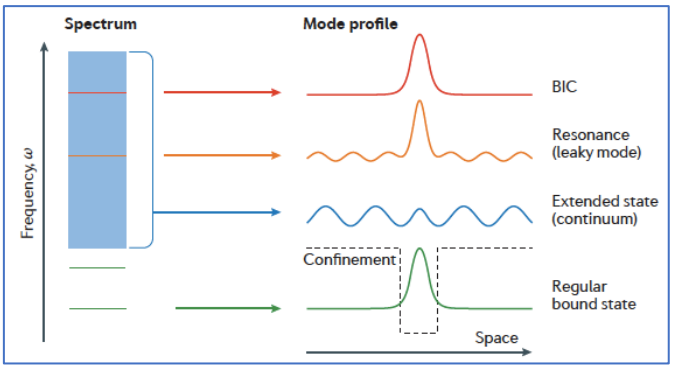

Figure 11: Illustration of a BIC in an open system (11).

- The green bounded state is representative of spatially confined waves, caused either by a confining structure in the system or an applied potential (the black dashed line).
- The blue wave shows the spectrum continuum, also known as the extended waves, which represents energy levels which tend to infinity, with almost negligible separation, so that they can be considered as one band of levels holding the same energy.
- The orange line shown the resonant waves earlier introduced; those whose frequency matches that of the continuum at infinity, thus enabling them to escape off as a transmission.
- The red wave portrays **the defiant BICs**; the one whose energy allows them to coexist with the continuous spectrum, but due to certain conditions, are unable to couple with the extended waves, thus allowing it (them) to stay localized with no radiation. Most theoretically proposed and all experimentally observed BICs are realized in ideal lossless extended (infinite) structures (such as periodic structures; the planar metasurface in this case).

If the leaky modes in a system are associated to an angular frequency $\omega = \omega_0 - j\gamma$, where ω_0 is the resonance frequency and γ is the leakage rate, it is easy to see that for a BIC, $\gamma = 0$.
The physical mechanisms leading to the formation of a BIC can be broadly categorized into several distinct types; those formed due to and shielded by the system symmetry or energy separability, those based on interference which yields trapped states, and those engineered through inverse construction (13).

A detailed description of the above categories is as listed below (11).

i). <u>Symmetry protected BICs</u>

Symmetry-protected BICs possess perfect energy confinement in the radiation continuum due to the symmetry incompatibility (14). As the definition suggests, the rotational or reflectional symmetry of the radiating system continuum differs from that of the selected mode, which is then prohibited from coupling to the continuum, if all factors defining the system's symmetry remain constant. An alternative consideration stems from the modification of given system parameters, thereby causing the said mode to decouple from the extended states, and due to the system's symmetry preservation after the variation, the BIC remains localised for as long as the conditions that led to its establishment are maintained.

ii). <u>BICs due to separability</u>

The first proposition of the definition of a symmetry protected BIC was by Robnik (15), who showed that the easiest way to portray or characterise them is by considering a 2D Hamiltonian system. Following this lead, Rivera et al. (16) not only portrayed the general characteristics of these BICs, but also demonstrated that they enable control over both the directionality and the dimensionality of resonantly emitted waves through symmetry exploitation.

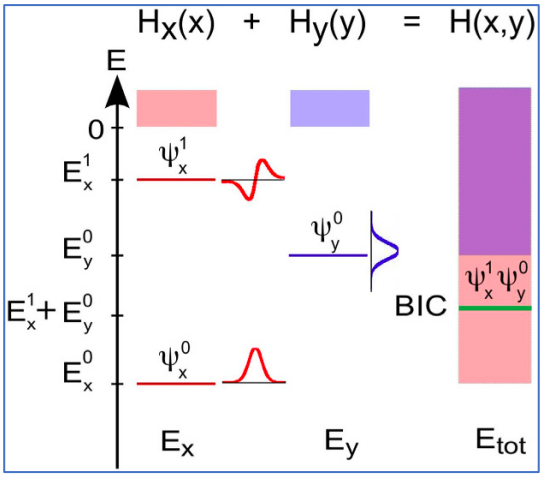

Figure 12: A 2D schematic demonstrating the concept of separable BICs. (16)

The system Hamiltonian $H(x,y)$, composed of the contributions in the x and y directions as shown, consisting of eigenstates $\Psi_x^i(x)$ and $\Psi_y^j(y)$ with energies E_x^i and E_y^j, is diagonalised by the product of the eigenstates and sum of the energies.

By assuming that H_x and H_y each have continua starting at zero energy, with at least one confined state, Ψ_x^0 and Ψ_y^0, respectively, then the continuum of the total Hamiltonian starts at $\left(\mathrm{E}_x^0, \mathrm{E}_y^0\right)$, derived from the ground states.

In the event that a bound state exists with $E^{i,j} > \left(\mathrm{E}_x^0, \mathrm{E}_y^0\right)$, it is a BIC. In the figure above, the separable system has H_x with two bound states, Ψ_x^0 and Ψ_x^1, while H_y has Ψ_y^0. The combination of the excited state in x and the ground state in y has a larger energy than the lowest continuum energy and is spatially bounded in both x and y, which makes it a BIC.

iii). BICs due to parameter tuning

Also known as interference based BICs, these result from the occurrence of destructive interference between different channels, as influenced by the enhancement of system parameters. The interfering channels could be resonances of different resonators, resonances of the same resonator, or even a single resonance.

a. Fabry-Pérot BICs

When a lossless resonant structure is coupled to a single radiation channel, its reflection reaches unity near the resonance frequency. If two of these resonators form a cavity at the resonance frequency, with a spacing d, by which the wave accumulates a cumulative phase shift that is an integral multiple of 2π, a destructive interference would form within the cavity. Following the coupled mode theory, in the absence of external driving sources, one of the eigen modes becomes a leaky resonance with twice the decay rate, while the other is presented as a BIC with a purely real eigenfrequency.

Fabry–Pérot BICs are commonly found in systems where two identical resonances are coupled to a single radiation channel.

A unique property of Fabry–Pérot BICs is that the two resonators interact strongly through radiation even when they are far apart.

b. Friedrich – Wintgen BICs

Contrary to the FP BICs, these BICs will occur when the separation is $d = 0$. The two resonances at the same location can lead to a BIC through interference of radiation, and unlike the former, unity reflection is not a requirement. Also, unlike the former, the two resonances have

differing resonant frequencies in the temporal coupled mode theory, and differing radiation rates.

One of the eigenvalues in the solution becomes purely real, hence a BIC, and the other becomes more lossy. Since these BICs are possible when the number of resonances exceeds the number of radiation channels, the required number of tuning parameters also grows with the number of radiation channels.

The spectral location of the FW BIC is generally near the frequency crossings of the uncoupled resonances.

c. Single-resonance parametric BICs

A single resonance can also evolve into a BIC when enough system parameters are tuned. The resonance itself is believed to originate from two or more waves, so that adjusting the system parameters supporting such a resonance can lead to suppression of radiation. This kind has not only been observed in Photonic Crystal slabs, but also periodic crystals, and their analysis is by spatial coupled wave theory.

Although these BICs are not guaranteed to exist by symmetry, when they do exist, they are robust to small changes in the system parameters, and their generation, evolution and annihilation follow strict rules that can be understood through the concept of topological charges.

These BICs can be described as **'topologically protected'** and are known to exist generically if the system parameters can be varied over a sufficient range.

iv). Quasi or near BICs

As expected from theoretical descriptions of BIC-supporting systems, the material ought to extend to infinite dimensions. However, in practice, due to the finite extent of structures, inherent material absorption, and other external perturbations, BICs collapse to what is known as a **Fano resonance**, with a limited radiative Q factor.

Such resonances are known as **quasi-BICs** and they have been used to obtain very high Q resonances in numerous photonic systems. They possess both finite lifetimes and large field enhancement inside the structures containing them (14).

Another type of high-Q resonances is called the **near-BIC**, which is obtained in the vicinity of a system BIC when it is detuned. Unlike BICs which are only attainable at a single value for a parameter change, these resonances can be obtained over an interval of values (13).

v). BICs built with inverse construction

As the name suggests, starting with a BIC, a possible system capable of supporting both the bounded state and its corresponding continuum is studied.

Inverse construction may generate non-physical or unrealizable systems, and therefore, the experimental realizations of such systems to date have been limited.

However, this method may offer a lot of promise for engineering and optimization of synthetic BICs in photonic systems.

a. Potential engineering

The introduction of the concept of BICs was set by von Neumann and Wigner, whose method was based on the amplitude modulation of a free-particle wave function, leading to an integrable eigenfunction produced by a local potential which was bounded and could be made to vanish at infinity (12). As an extension of their formulism, Stillinger and Herrick set to correct their algebraic error and establish by principle that the alterations in the system parameters change the potential and ultimately destroy the BIC, unless the potential variation either maintained a long-range oscillatory character or was consistent with an eigenvalue linked to its associated wave vector (17).

Much as potential engineering allows for analytic solutions of the BICs, we see that the obvious disadvantage is that it yields unrealistic systems.

b. Hopping rate engineering

The hopping rate between the nearest neighbours within a tight binding lattice model was realised by Corrielli et al (18) in a coupled optical waveguide array, in which it was tuned by the distance between neighbouring waveguides. For a semi-infinite 1D lattice with a constant on-site energy and a hopping rate κ_n between sites n and $n+1$,

$$\kappa_n = \begin{cases} \kappa & n \neq lN \\ \left(\frac{l+1}{l}\right)^{\beta} \kappa & n = lN, (l = 1,2,3 \dots) \end{cases}$$

With $N > 1$ as an integer, $\beta > 1/2$ as an arbitrary real number, κ as the reference hopping rate, the system would support $(N-1)$ BICs localized near the surface $(n = 1)$.

Green function for point dipole sources

The Dyadic Green function $\overleftrightarrow{\boldsymbol{G}}$ describe the electric field $\boldsymbol{E}$, at a point $\boldsymbol{r}$ in space, generated by a radiating electric dipole $\boldsymbol{p}$, located at the source point $\boldsymbol{r'}$, given by the expression below.

$$\mathbf{E}(\mathbf{r}) = \omega^2 \mu_0 \mu \, \overleftrightarrow{\mathbf{G}}(\mathbf{r}, \mathbf{r}')\mathbf{p}$$

Regarding an inherent sphere homogeneity $\delta(\mathbf{r} - \mathbf{r}')$ which is always 0 except when $\mathbf{r} = \mathbf{r}'$, we have a linear equation which leads to the derivation of the Green function reading as

$$\mathcal{L}\, \overleftrightarrow{\mathbf{G}}_{\boldsymbol{i}}(\mathbf{r}, \mathbf{r}') = \boldsymbol{n}_i \delta(\mathbf{r} - \mathbf{r}'), \qquad (i = x, y, z)$$

Where $\boldsymbol{n}_i$ is a constant unit vector, $\overleftrightarrow{\mathbf{G}}_{\boldsymbol{i}}(\mathbf{r}, \mathbf{r}')$ is the solution to the linear operator $\mathcal{L}$ acting on the source $\boldsymbol{n}_i \delta(\mathbf{r} - \mathbf{r}')$, and $\mathbf{r}'$ is the location of the inhomogeneity.

In closed form, the above 3 equations can be written as

$$\mathcal{L}\, \overleftrightarrow{\mathbf{G}}\,(\mathbf{r}, \mathbf{r}') = \overleftrightarrow{\mathbf{I}}\, \delta(\mathbf{r} - \mathbf{r}')$$

The linear operator $\mathcal{L}$ separately acts on each column of $\overleftrightarrow{\mathbf{G}}$, which is the dyadic Green function, and $\overleftrightarrow{\mathbf{I}}$ is the unit dyad.

The Green function for the electric field is derived similarly to the inhomogeneous Helmholtz equation, by the introduction of an electromagnetic vector potential and a Lorentz gauge. Further details pertaining to this derivation can be found in the book used as the reference (19). The dyadic Green function can eventually be calculated from the scalar Green function G_0 as

$$\overleftrightarrow{\mathbf{G}}\,(\mathbf{r}, \mathbf{r}') = \left[\overleftrightarrow{\mathbf{I}} + \frac{1}{\mathrm{k}^2} \nabla\nabla\right] \mathrm{G}_0(\mathbf{r}, \mathbf{r}')$$

With $\overleftrightarrow{\mathbf{I}}$ standing for the unit dyad (unit tensor), the columns in the tensor $\overleftrightarrow{\mathbf{G}}$ corresponding to the field due to a point source in the x, y and z directions respectively, k representing the wave number, and $\nabla\nabla$ stemming from the expression of the gradient of a divergence of the vector field as applied to $\nabla \cdot \left[\mathrm{G}_0 \overleftrightarrow{\mathbf{I}}\right] = \nabla \mathrm{G}_0$

CEMD formalism

The coupled dipole equations for periodic spherical silicon particles are helpful in the analysis of the material's optical response features and local electromagnetic fields. The model accounts for the electric and magnetic dipole moments of the particles embedded in a homogeneous dielectric medium (8). It should be noted that the coupled dipole theory is valid when the periodicity is greater than the particle dimensions.

Abujetas et al. derived a coupled electric and magnetic dipole (CEMD) analytical formulation for the description of the reflection and transmission occurrence in planar metasurfaces (20). In their paper, they show by analysis the reflection and transmission in 2D lattices of the in and out of plane electric and/ magnetic dipolar resonances for the nanoparticles under consideration.

Their enhancement to the pre-existing CEMD implementations was not only wrapped around re-writing the 2D lattice Green function in 1D for ease of computation, rather than numerical extraction through convergence, but also analysis of the lattice modes associated to the poles of the same Green function. This thesis specifically looks into the specular diffractive order case for a planar all-dielectric silicon nanospheres' metasurface, whose BICs and resonances are easily attained from the above mentioned poles.

To note (8):

i) Through the Mie theory, an effective combination between the electric and magnetic field polarizabilities for an arbitrary sphere is applicable to the coupled-dipole method.

ii) The optical response and local field distributions strongly depend on the particle size and shape, the interaction between subsequent neighbouring particles, and the polarisation of the incident field.

iii) The coupled dipole theory is valid when the periodicity is greater than the particle dimensions.

Light transmission of finite-size arrays of Si particles can be significantly suppressed at the conditions of the particle magnetic dipole resonance. Using resonant conditions, one can separately control the enhancements of local electric and magnetic fields in the structures. In that case, each particle is treated as a dipole scatterer and the total dipole moments of the particles are found by solving the coupled dipole equations, including the cases where particles are considered as electric and magnetic dipoles (8).

IMPLEMENTATION OF THE CEMD FORMALISM

Nanospheres' metasurface

3.1.1 Reproducing results

Results for the reflectance as obtained using the initial CEMD formulation (20) were reproduced in this study, from the direct generation of the electric field complex amplitude quantities in reflection and transmission.

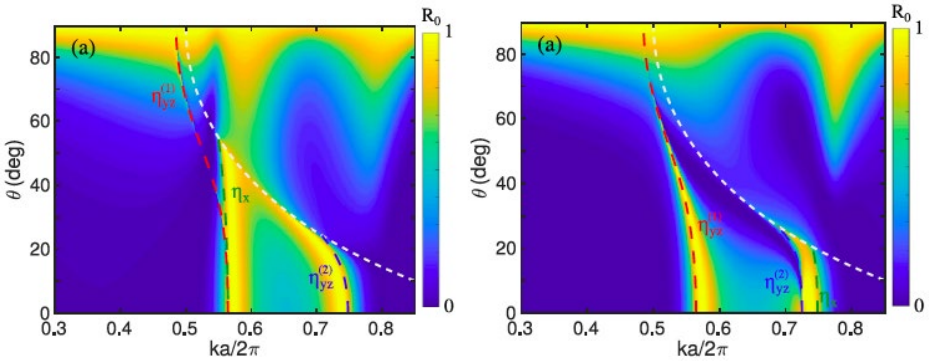

Figure 13: Colour maps for TE and TM reflectance (left and right) for the square array of dielectric nanospheres (20).

The plots of the real components of the said amplitudes were plotted, corresponding to both reflectance and transmittance, which show negligible absorption losses, as expected.

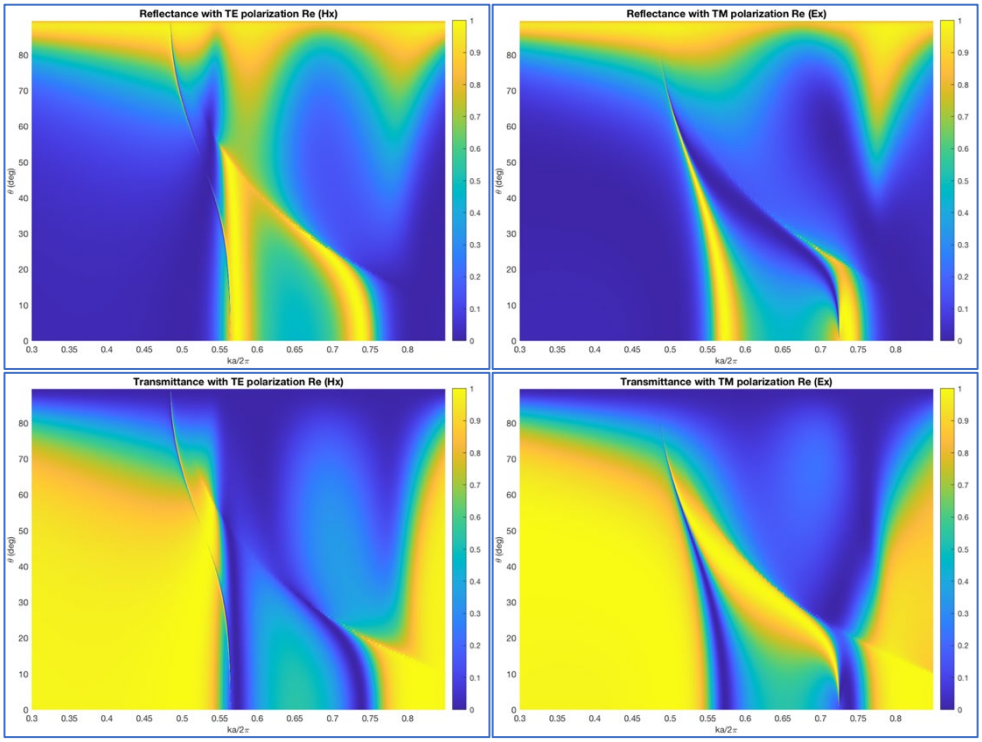

Figure 14: Reproduction of the TE and TM polarisation plots in reflection from (20) with the corresponding counterpart in transmission.

Due to the nature of the metasurface, it is transparent at all points of normal incidence, as witnessed by the reflectance and transmittance plots above, except for the region between the dimensionless frequency expression $\frac{ka}{2\pi} = 0.53$ and 0.78, which contains the resonance bands in which the MS is completely opaque to the impinging field.

As stated before, k stands for the wave number, and a for the lattice periodicity of the MS.

With focus on the plots in reflection, knowledge of the fact that the impinging beam propagates from air to the HRI metasurface indicates external reflection in both polarisation cases. However, at normal incidence, this value is always 0 outside the resonance bands. As the value of the angle of incidence grows (still considering the regions outside resonance), the MS is transparent until after 70°, and eventually, we see 100% reflection at grazing incidence. The region of interest is that which is below the diffraction limit (the nondiffracting region), as delimited by the white dashed lines in figure 13.

The resonance bands delimited by the ranges $\frac{ka}{2\pi} = 0.55 - 0.60$ and $\frac{ka}{2\pi} = 0.72 - 0.76$ correspond to the MD and ED resonances respectively, since from the Mie theory of (specifically HRI) dielectric scatterers the first spectral resonance from the side of large wavelengths always corresponds to the magnetic dipole term (8).

3.1.2 Normalising the field components

Prior to investigation of the impact of the MS on a change in polarisation, we studied the real and imaginary parts of the transverse components' reflection and transmission coefficients.

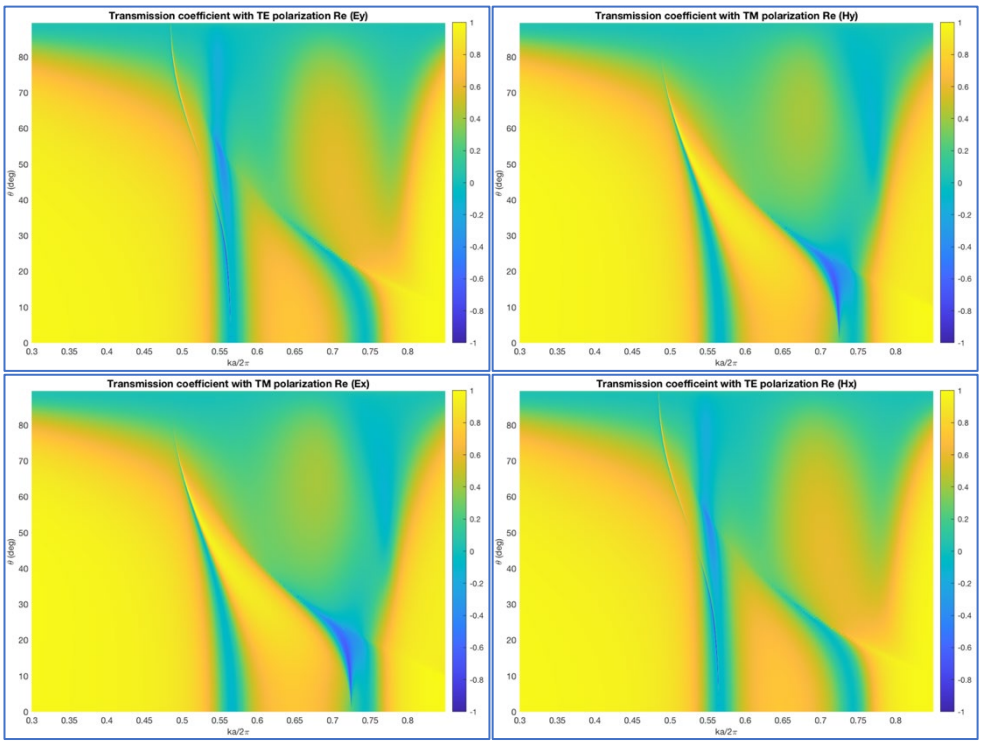

Figure 15: TE and TM polarization real parts of the transmission coefficient

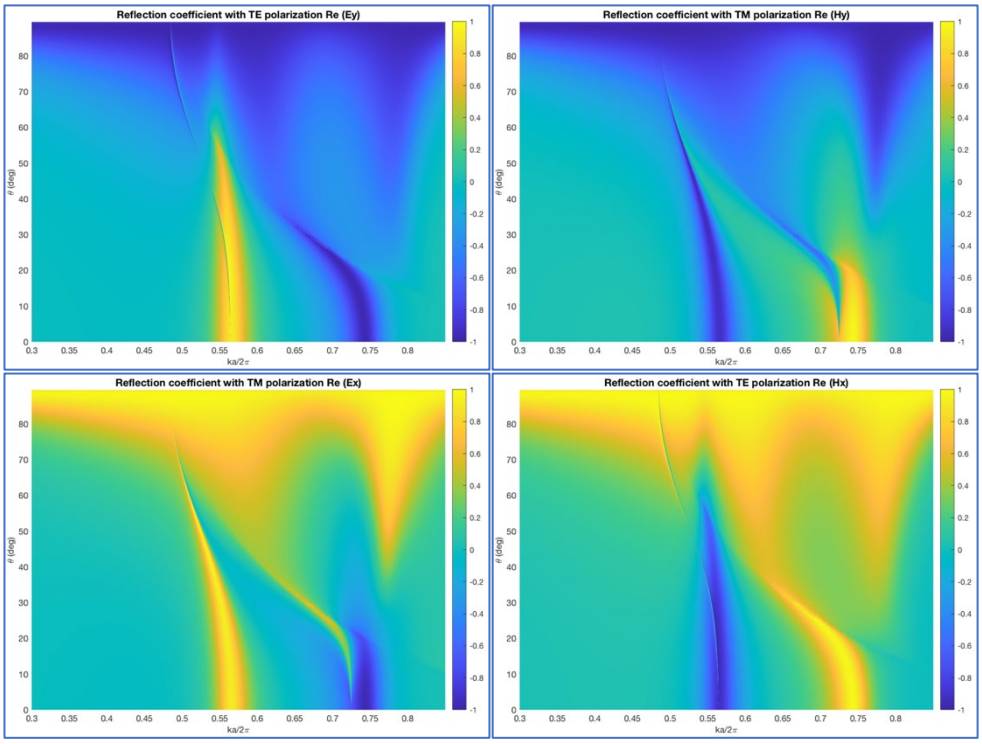

Figure 16: TE and TM polarization real parts of the reflection coefficient

The contribution from the imaginary parts of the reflection and transmission coefficients is not displayed here, albeit being computed, because it makes no significant impact on the discussion, because the explanation is exactly the same.

As observed, for the real part of the transmission coefficient, the E_y matched H_x for TE polarisation, and the E_x matches the H_y for the TM polarisation. For the case of reflection, the same holds true, although the polarity is opposite (as expected). However, because of the right-hand rule, we normalised the electric field amplitude components in both reflection and transmission as follows;

Both the reflected and transmitted E_y field components were normalised with a factor of (-1) for TE polarisation , whereas only the reflected field's H_y component in TM polarization was normalised in the same way. The motivation for this choice of actions will further be expounded on in the next section.

Upon completion of the normalisation, we considered the TE and TM electric fields, and after introducing a phase shift, we had circularly polarised light, as well as oblique linearly polarised light, whose Stokes parameters were then fully obtained.

RESULTS AND DISCUSSION

Nano spheres' implementation

4.1.1 Introduction

In this chapter, we introduce the Stokes parameters, earlier discussed in the literature review, as they're applied to the electric field amplitude components, in order to study the effects of a variation in polarisation of incident waves on the all-dielectric metasurface.

Drawn from the CEMD formalism, the attained Electric field component values in reflection and transmission respectively are given as 6*1 column vectors of the form

$$E_{r,t}(TE,TM) = \begin{bmatrix} E_x \\ E_y \\ E_z \\ ZH_x \\ ZH_y \\ ZH_z \end{bmatrix}$$

Where Z is the impedance of the nano resonators, given as $\sqrt{\frac{\mu}{\varepsilon}}$

The individual components used to generate the Stokes' plots were $R_{TE} = \frac{E_{y,r}}{-1}$, $T_{TE} = \frac{E_{y,t}}{-1}$, $R_{TM} = \left(H_{y,r} * -1\right)$, and $T_{TM} = \left(H_{y,t}\right)$, where $E_{y,r/t}$ and $H_{y,r/t}$ stand for the electric and magnetic field components in the y direction respectively, for the reflected or transmitted field.

The value (-1) was used to normalise the field for both polarisation cases impinging the metasurface. Since the incident electric field for TE polarisation was inherently negative, the purpose of the normalisation was to ensure that the incorrect sign doesn't negatively impact the results.

For TM polarisation on the other hand, preference is given to the magnetic over electric field, which only means that the H_y field was preferred for convenience. Since its sign is opposite to that of the electric field, the sign change to the reflected component (only) would ease the computation of the Stokes parameters.

With this information, the Stokes parameters were generated as shown below, and plotted for the selected spectrum. The values below correspond to the values for the reflected field, but equivalent substitution yields components for the transmitted field.

$$I = |R_{TE}|^2 + |R_{TM}|^2$$
$$Q = |R_{TE}|^2 - |R_{TM}|^2$$
$$U = 2Re\{R_{TE}^* R_{TM}\}$$
$$V = 2Im\{R_{TE}^* R_{TM}\}$$

Specific considerations made for the RHCP, LHCP, +45° LP and -45° LP in this thesis are shown below for all the cases, with $R_{TE\_initial}$ and $R_{TM\_initial}$ representing the normalised field components, each of which is treated with the factor shown below, to enable the conversion to the desired state of polarisation.

Right handed circular polarisation:

$$R_{TE} = \frac{1}{\sqrt{2}} * R_{TE\_initial}$$
$$R_{TM} = \frac{1}{j\sqrt{2}} * R_{TM\_initial}$$

Left handed circular polarisation:

$$R_{TE} = \frac{1}{\sqrt{2}} * R_{TE\_initial}$$
$$R_{TM} = \frac{1}{-j\sqrt{2}} * R_{TM\_initial}$$

+45° Linear polarisation:

$$R_{TE} = \frac{1}{\sqrt{2}} * R_{TE\_initial}$$
$$R_{TM} = \frac{1}{\sqrt{2}} * R_{TM\_initial}$$

-45° Linear polarisation:

$$R_{TE} = \frac{1}{\sqrt{2}} * R_{TE\_initial}$$
$$R_{TM} = \frac{1}{-\sqrt{2}} * R_{TM\_initial}$$

4.1.2 Graphical representation of the results

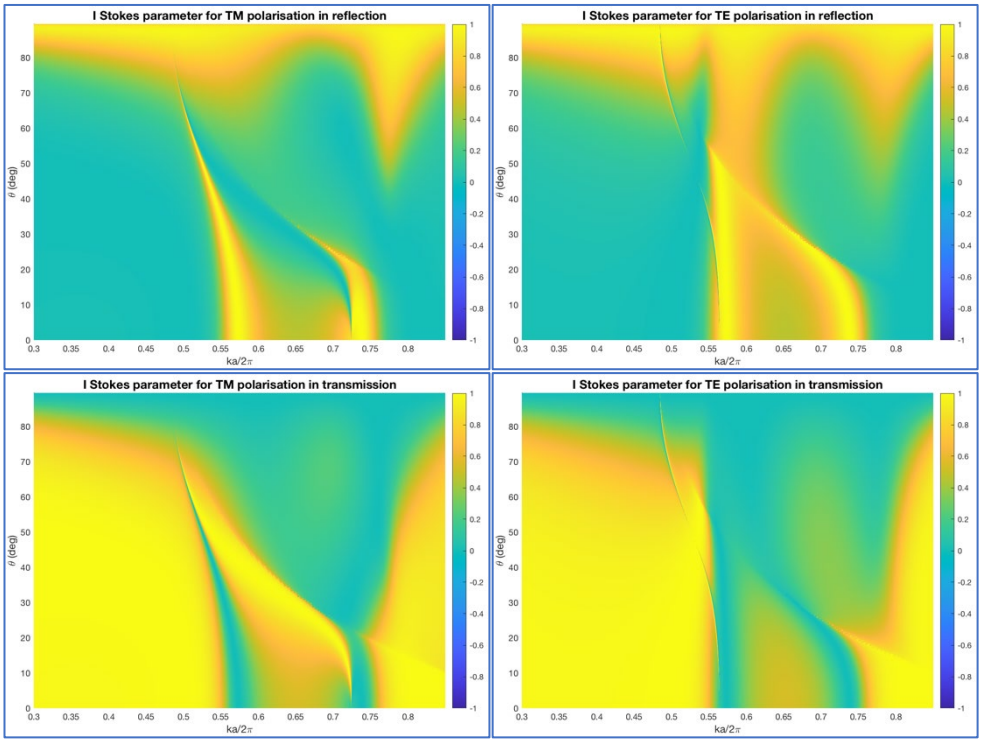

Figure 17: I Stokes parameters for TE and TM polarisation in reflection and transmission

The explanation doesn't deviate from that given at the introduction of chapter 3, as the contribution from the TE or TM component is multiplied by 0 for the assessment of the other.

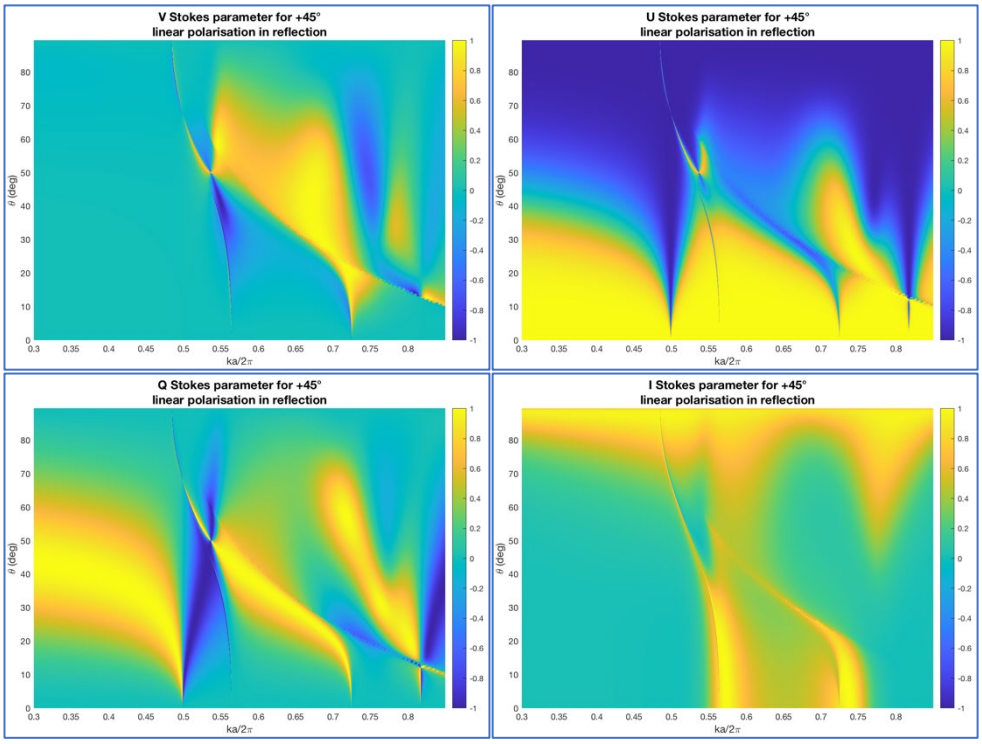

Figure 18: Stokes parameters for +45° linear polarization in reflection

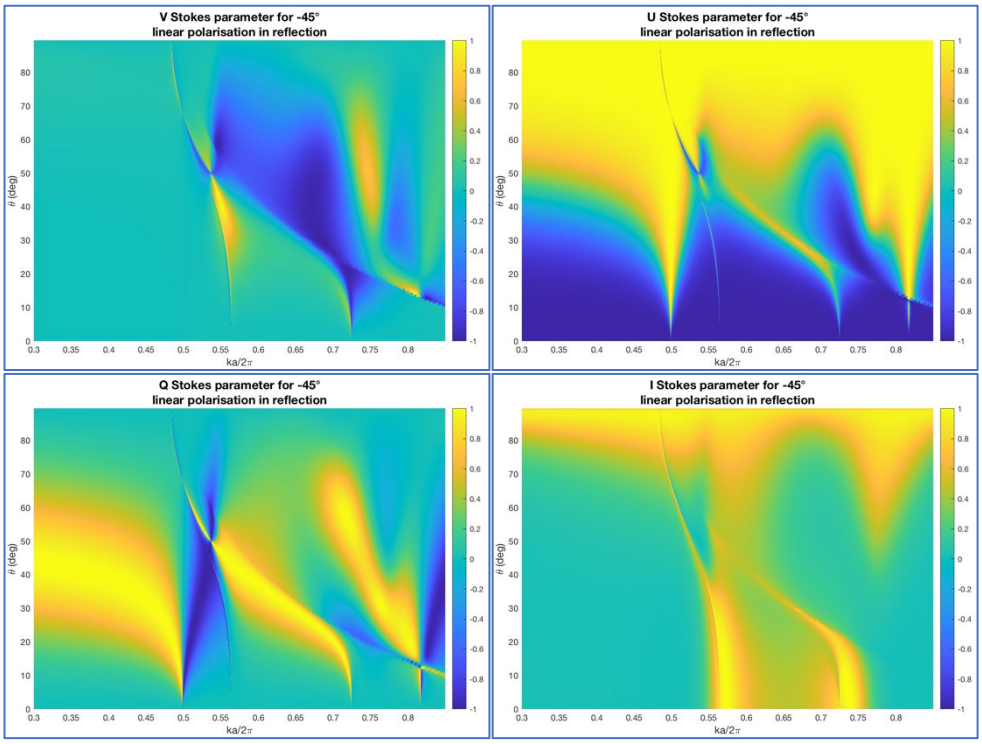

Figure 19: Stokes parameters for -45° linear polarization in reflection

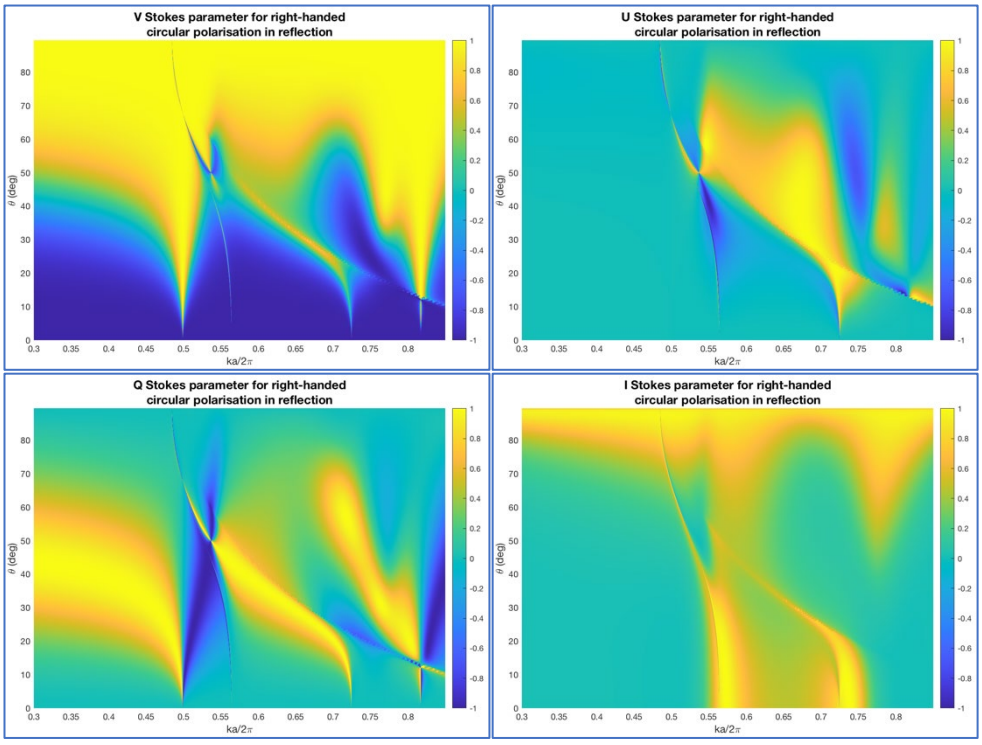

Figure 20: Stokes parameters for right-handed circular polarization in reflection

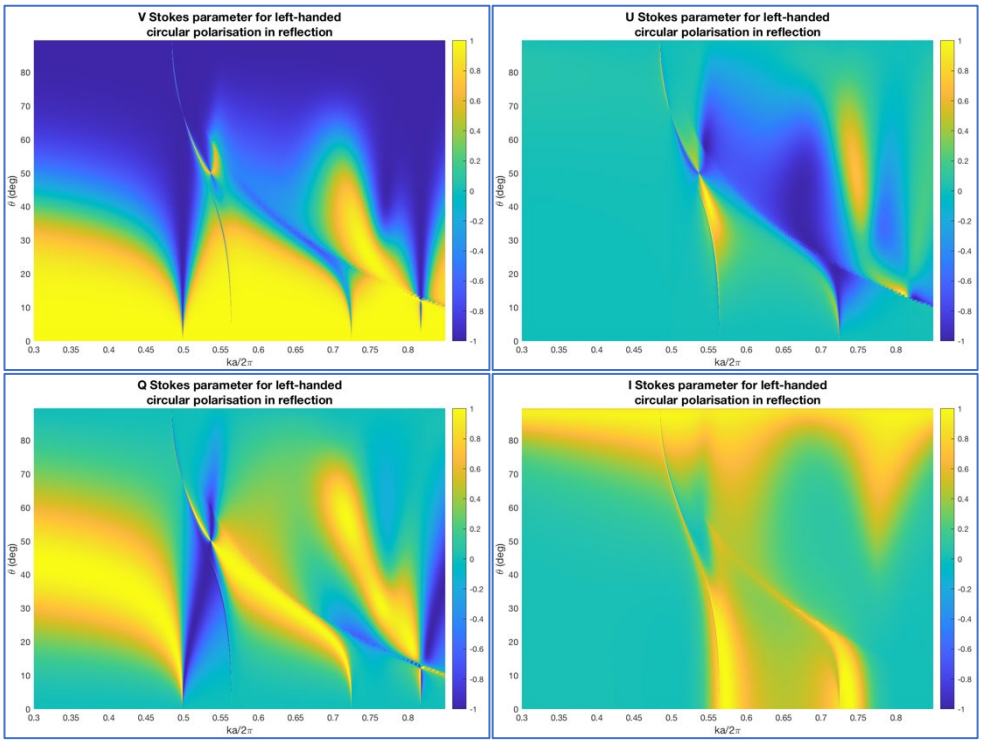

Figure 21: Stokes parameters for left-handed circular polarization in reflection

The I and Q Stokes' parameters for +45° and -45° linear polarisation, as well as left-handed and right-handed circular polarisation are exact replicas of each other, which makes obvious sense, given the computation involved in obtaining them.

The difference only lies in the fact that the U and V parameters swap, given that the U parameter considers the real part, while the V parameter considers the imaginary part of the complex amplitudes as shown in the expression, which causes the U Stokes parameter for +45° polarisation to be equal to the V Stokes parameter for left-handed polarisation, the U Stokes for -45° to be equal to the V Stokes for right-handed circular polarisation, and the same is true for the other two cases.

It should be noted that the only regions relevant to the discussion are those confined between $\frac{ka}{2\pi} = 0.5 - 0.8$, but since the plots above were normalised by I to better enhance the structure of the features to be studied, it might be misleading to assume that the parts outside this range hold any relevant significance.

Considering the plots in transmission, whose features are better enhanced than the former,

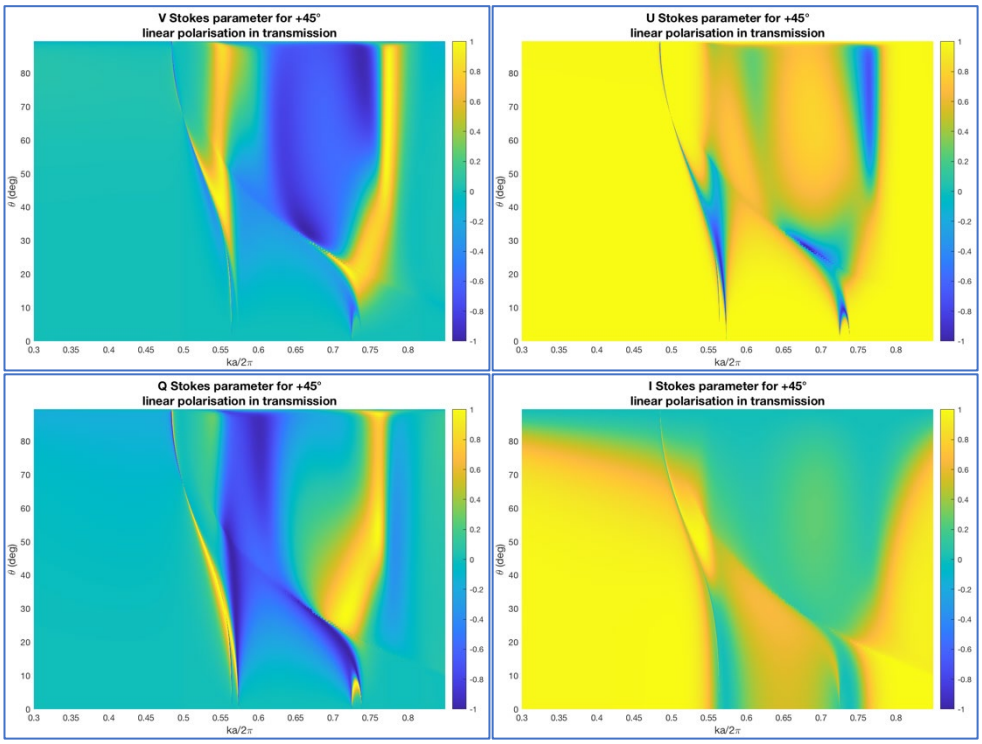

Figure 22: Stokes parameters for +45° linear polarization in transmission

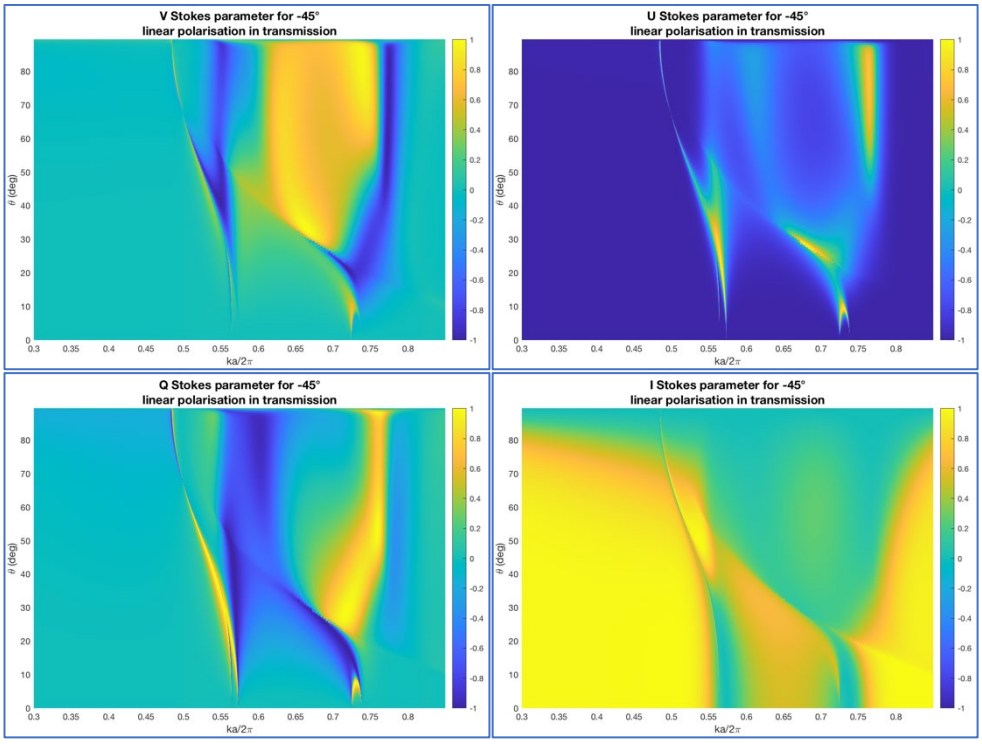

Figure 23: Stokes parameters for -45° linear polarization in transmission

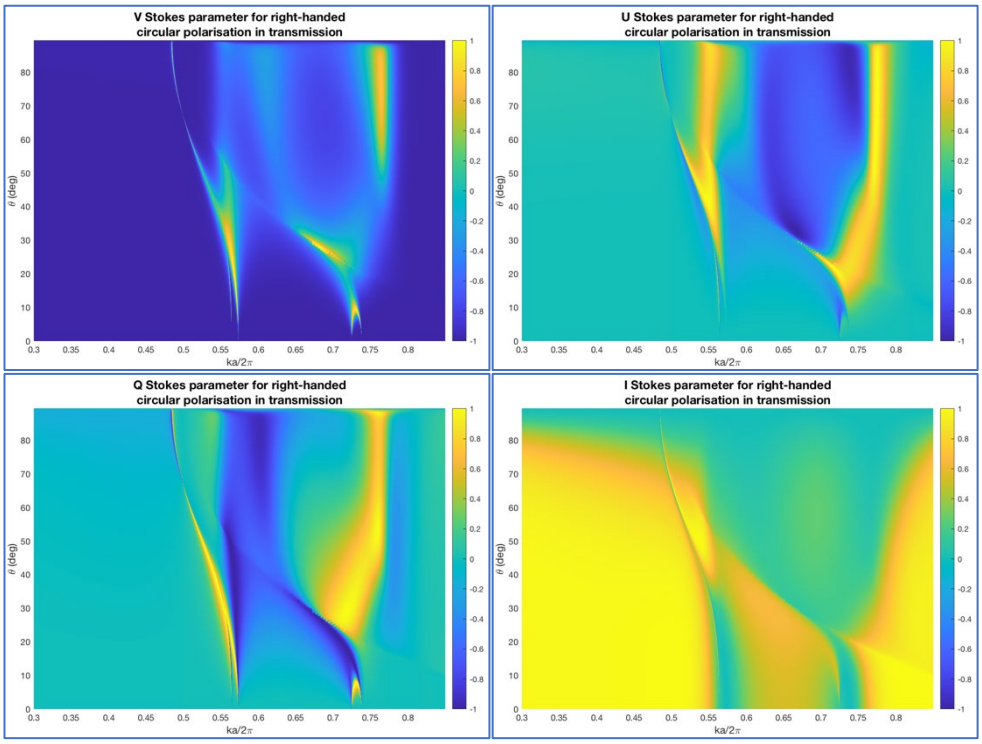

Figure 24: Stokes parameters for right-handed circular polarization in transmission

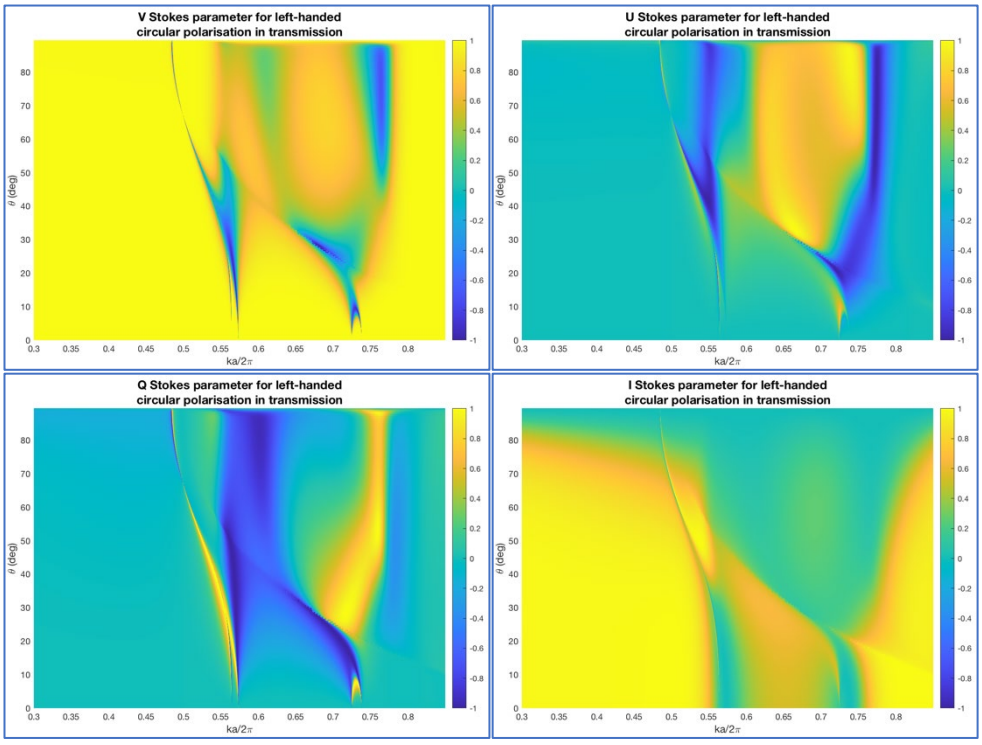

Figure 25: Stokes parameters for left-handed circular polarization in transmission

Considering all other factors constant, we ascertained that it is sufficient to explain the characteristics of the metasurface in terms of its Stokes parameters by considering one case, due to the obvious interconnections among them all.

By zooming in to the case of LHCP in transmission as shown,

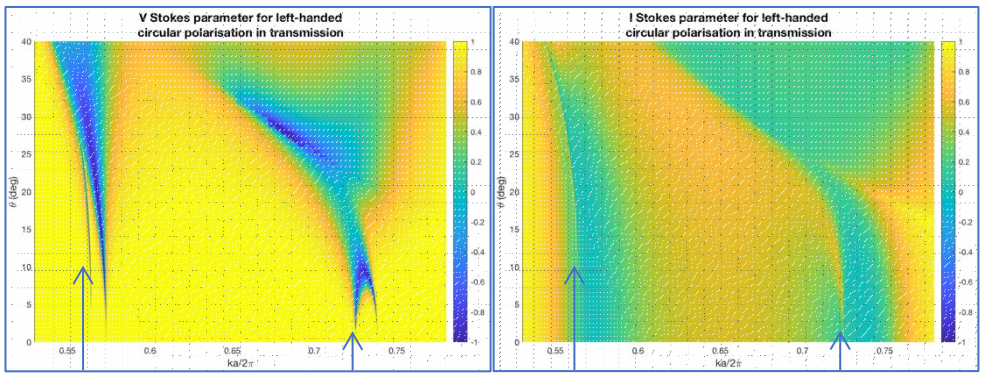

Figure 26: The resonant regions for left-handed circular polarisation in transmission

Considering the grid-annotated plots for the V and I Stokes parameters in transmission for left-handed circular polarisation, we see that there is confirmation of the existence of the BICs as described here (20).

The arrows represent the regions within the resonance bands with transmission, comparing with the I Stokes parameter to show what effects from the V should be ignored (those in regions with 0 transmission).

The BICs present themselves at approximately $\frac{ka}{2\pi} = 0.57$ and 0.73 respectively (by visual inspection) for the lower and higher frequency resonance bands respectively.

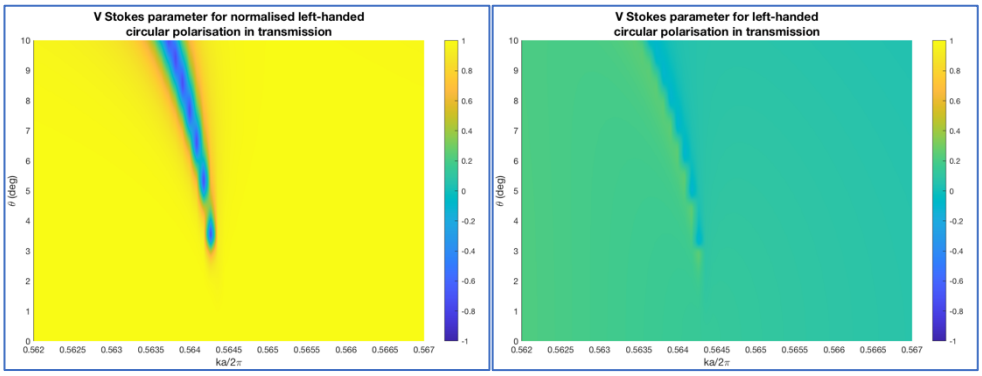

Figure 27: Visualising the lower-frequency BIC region by the V Stokes parameter

The BIC presented in this region comes from the magnetic dipole oscillations, and it presents close to normal incidence (at 3° to be precise).

It is protected by the symmetry of the nanospheres' square lattice. It is initially narrow, but broadens with greater angles of incidence, fully diverging at the diffraction limit.

We see that with about 20% of intensity of the incoming power, we have close to 70% polarisation conversion efficiency of the bounded state, as depicted by the colour bar scales on each of the plots in I and V (figure 28 below).

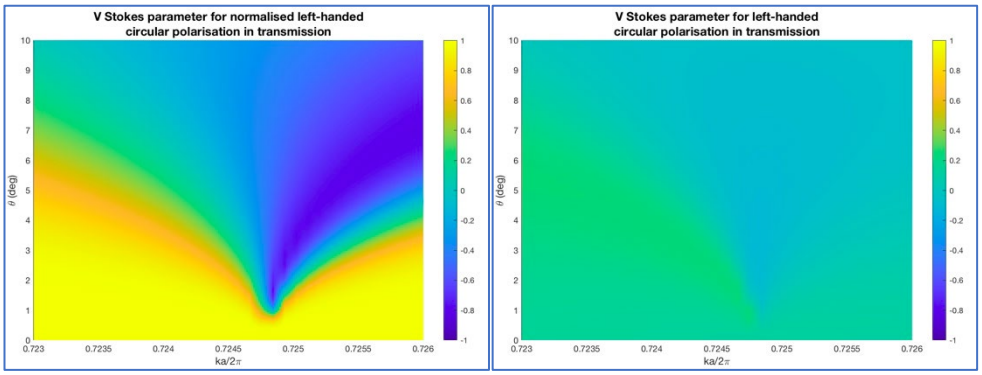

Figure 28: Visualising the higher-frequency BIC region by the V Stokes parameter

Closer to normal incidence, this band presents a BIC due to the vertical electrical dipole oscillations, which broadens with larger angles of incidence. We also see from the normalised plot for the V Stokes parameter (figure 28) in this case that with about 80% intensity (refer to the same point for the I Stokes parameter plot on figure 26), we have close to 100% polarisation conversion efficiency.

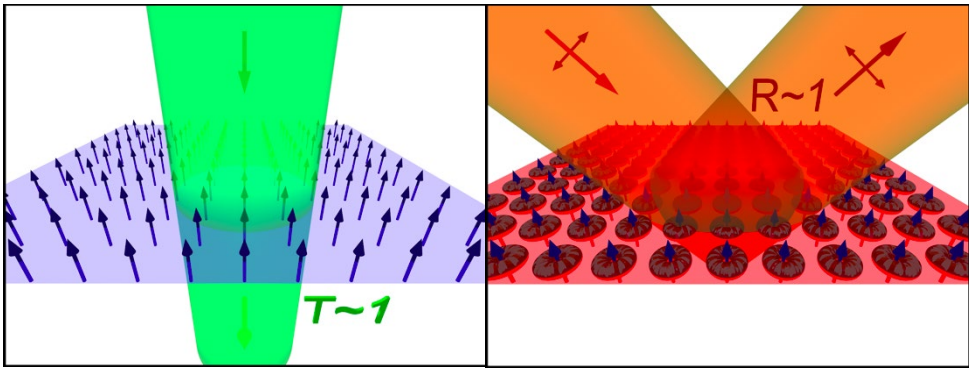

Figure 29: Represent of vertical dipoles in the array

Figure 29 above shows plots corresponding to the vertical dipoles observed in a nanodisk array (21), and this thesis considers nanospheres which similarly present in-plane dipoles.

The analysis in our implementations differs from the above because upon excitement, a nanospheres array scatters light that overlaps with the vertical dipole BIC, so that close to normal incidence, the BIC is invisible because all the light is reflected by the in-plane dipoles.

Nearly all light is transmitted at the quasi-BIC (further away from normal incidence) due to the interference imposed by the Fano resonance between the vertical-dipole quasi-BIC and the broad in-plane resonant band.

CONCLUSIONS

The developed CEMD analytical formulation was useful for the description of the reflection and transmission characterisation of this all-dielectric metasurface of electric and/or magnetic particles, for the specular diffraction consideration, and showed important characteristics as are shown below;

Much as the BICs initially present as symmetry protected (close to normal incidence), with further perturbations in the system, the limitations presented by the infinite dimensions of the metasurface (500 nanospheres considered in this study) and cumulative subsequent absorption losses (albeit negligible in magnitude), they are converted into quasi BICs, which present a characteristic asymmetry in the resonance bands, which when excited can be attributed to Fano resonances.

The fact that the BICs present themselves in the same expected positions, even though the impinging field's polarisation is altered to either circular or 45° oblique incidence is indicative of the successful use of the metasurface to achieve polarisation conversion.

To note: The use of CP light is useful to address issues like multipath fading, Faraday rotation and depolarisation for a propagating wave. This makes it particularly useful in antenna alignment, as well as the setup of transmitting and receiving antennas (21). Application of this method would be very helpful in such setups and scenarios.

Works Cited

1. Bahaa E. A. Saleh, Malvin Carl Teich. *Fundamentals of Photonics.* Hoboken, New Jersey : Wiley-Interscience, 2007.

2. Wenshan Cai, Vladimir Shalaev. *Optical Metamaterials, Fundamentals and Applications.* New York : Springer, 2010.

3. *Dielectric Meta-Reflectarray for Broadband Linear Polarization Conversion and Optical Vortex Generation.* Yuanmu Yang, Wenyi Wang, Parikshit Moitra, Ivan I. Kravchenko, Dayrl P. Briggs, Jason Valentine. 3, 2014, Nano Letters, Vol. 14, pp. 1394-1399.

4. *Integrating polarization conversion and nearly perfect absorption with multifunctional metasurfaces.* Cheng Hua, Wei Xiaoyun, Yu Ping, Li Zhancheng, Liu Zhe, Li Junjie, Chen Shuqi, Tian Jianguo. 17, 2017, Applied Physics Letters, Vol. 110.

5. *Optically resonant dielectric nanostructures.* Arseniy I. Kuznetsov, Andrey E. Miroshnichenko, Mark L. Brongersma, Yuri S. Kivshar, Boris Luk'yanchuk. 6314, 2016, Science, Vol. 354.

6. *All-dielectric meta-optics and non-linear nanophotonics.* Kivshar, Yuri. 2018, National Science Review, Vol. 5, pp. 144–158.

7. *Magneto-Optical Response Enhanced by Mie Resonances in Nanoantennas.* Maria G. Barsukova, Alexander S. Shorokhov, Alexander I. Musorin, Dragomir N. Neshev, Yuri S. Kivshar,Andrey A. Fedyanin. 10, 2017, ACS Photonics, Vol. 4, pp. 2390-2395.

8. *Optical response features of Si-nanoparticle arrays.* Andrey B. Evlyukhin, Carsten Reinhardt, Andreas Seidel, Boris S. Luk'yanchuk, Boris N. Chichkov. 4, 2010, Physical Review B, Vol. 82.

9. *Fano resonances in photonics.* Mikhail F. Limonov, Mikhail V. Rybin, Alexander N. Poddubny, Yuri S. Kivshar. 2017, Nature Photonics, Vol. 11, pp. 543–554.

10. *Functional Meta-Optics and Nanophotonics Governed by Mie Resonances.* Sergey Kruk, Yuri Kivshar. 11, 2017, ACS Photonics, Vol. 4, p. 2638−2649.

11. *Bound states in the continuum.* Chia Wei Hsu, Bo Zhen, A. Douglas Stone, John D. Joannopoulos & Marin Soljačić. 2016, Nature Reviews Materials, Vol. 1.

12. John von Neumann, Eugene Paul Wigner. Über merkwürdige diskrete Eigenwerte. *The Collected Works of Eugene Paul Wigner.* Berlin, Heidelberg : Springer, 1993, pp. 291-293.

13. *Photonic Bound States in the Continuum: From Basics to Applications.* Shaimaa I. Azzam, Alexander V. Kildishev. 1, 2020, Advanced Optical Materials, Vol. 9.

14. *Symmetry-protected bound states in the continuum supported by all-dielectric metasurfaces.* Shiyu Li, Chaobiao Zhou, Tingting Liu, Shuyuan Xiao. 6, 2019, PHYSICAL REVIEW A, Vol. 100.

15. *A simple separable Hamiltonian having bound states in the continuum.* Robnik, Marko. 1986, Journal of Physics A: Mathematical and General, Vol. 19, pp. 3845-3848.

16. *Controlling Directionality and Dimensionality of Radiation by Perturbing Separable Bound States in the Continuum.* Nicholas Rivera, Chia Wei Hsu, Bo Zhen, Hrvoje Buljan, John D. Joannopoulos, Marin Soljačić. 1, 2016, Scientific Reports, Vol. 6.

17. *Bound states in the continuum.* Frank H. Stillinger, David R. Herrick. 2, 1975, PHYSICAL REVIEW A, Vol. 11.

18. *Observation of Surface States with Algebraic Localization.* G. Corrielli, G. Della Valle, A. Crespi, R. Osellame, S. Longhi. 22, 2013, Physical Review Letters, Vol. 111.

19. Rautio, James C. IEEE Spectrum. [Online] 1 December 2014. [Cited: 13 July 2021.] https://spectrum.ieee.org/tech-history/dawn-of-electronics/the-long-road-to-maxwells-equations.

20. *Coupled electric and magnetic dipole formulation for planar arrays of particles: Resonances and bound states in the continuum for all-dielectric metasurfaces.* Diego R. Abujetas, Jorge Olmos-Trigo, Juan J. Sáenz, and José A. Sánchez-Gil. 12, 2020, Physics Review B, Vol. 102.

21. *Brewster quasi bound states in the continuum in all-dielectric metasurfaces from single magnetic- dipole resonance meta-atoms.* Diego R. Abujetas, Ángela Barreda, Fernando Moreno, Juan J. Sáenz, Amelie Litman, Jean-Michel Geffrin, José A. Sánchez-Gil. s.l. : Nature Scientific reportr, 2019, Vol. 9.

22. Lukas Novotny, Bert Hecht. *Principles of Nano-Optics.* Cambridge : Cambridge University Press, 2012.

23. Max Born, Emil Wolf. *Principles of Optics.* Cambridge : Cambridge University Press, 1999.

24. *Studies on polarizabilities and scattering behavior of small spherical particles.* Reena Sharma, Ari Sihvola. 2000, Radio Science, Vol. 5, pp. 83-89.

25. *Metamaterial-inspired silicon nanophotonics.* Isabelle Staude, Jörg Schilling. 5, 2017, Nature Photonics, Vol. 11, pp. 274-284.

26. *Flat optics with designer metasurfaces.* Yu Nanfang, Capasso Federico. 2014, Nature Materials, Vol. 13, pp. 139-150.

27. *Electronic control of linear-to-circular polarization conversion using a reconfigurable metasurface.* 21, 2017, Applied Physical letters, Vol. 111.
28. *High-Efficiency Dielectric Huygens' Surfaces.* Manuel Decker, Isabelle Staude, Matthias Falkner, Jason Dominguez, Dragomir N. Neshev, Igal Brener, Thomas Pertsch, Yuri S. Kivshar. 6, 2015, Advanced Optical Materials, Vol. 3, pp. 813-820.
29. *Mie resonance-based dielectric metamaterials.* Qian Zhao, Ji Zhou, Fuli Zhang, Didier Lippens. 12, 2009, Mateials Today, Vol. 12, pp. 60-69.
30. *Global Mie Scattering: Polarization Morphologies and the Underlying Topological Invariant.* Chen Weijin, Yang Qingdong, Chen Yuntian, Liu Wei. 23, 2020, ACS Omega, Vol. 5, p. 14157−14163.
31. —.Weijin Chen, Qingdong Yang, Yuntian Chen, Wei Liu. 23, 2020, ACS Omega, Vol. 5, pp. 14157-14163.
32. Buschow, Kurt Heinz Jürgen. *Handbook of Magnetic Materials.* Amsterdam : Elsevier, 2016.
33. *Directional visible light scattering by silicon nanoparticles.* Yuan Hsing Fu, Arseniy I. Kuznetsov, Andrey E. Miroshnichenko, Ye Feng Yu, Boris Luk'yanchuk. 1, 2013, Nature Communications, Vol. 4.

ACKNOWLEDGEMENTS:

Being granted the opportunity to work at Instituto de Estructura de la Materia under the Spanish national research council has been nothing short of a great pleasure and absolute honour. My motivation was the desire to do nano phonics-related research, as motivated by prof. Domenico de Ceglia, who was incidentally my thesis supervisor. Filling in for him is Prof. Marco Santagiustina, whose invaluable contribution to the completion of my thesis cannot go unnamed.

Prof. Domenico guided my deeper understanding of the topics discussed through my internship mobility program, by availing and suggesting literature to use to follow the brand new topics to which I was introduced in March 2021. Prof. Santagiustina has helped fine-tune my thesis and given me intriguing and interesting questions to follow, to enable me to better understand photonic BICs.

It goes without saying that I extend my absolute sincere gratitude to prof. José Antonio Sanchez-Gil who has greatly mentored me in the topics particularly related to responses from impinging fields on metasurfaces. Additionally, I am very grateful to Dr. Diego Ramirez Abujetas, prof. José's former PhD. Student, who worked tirelessly to help me get a better grip on the concepts of the programming language used during this internship period. They have both been readily available to clear out my doubts, despite their endlessly busy schedules.

I can safely say that despite the turbulence involved, I have an even more pronounced desire to pursue research as a career path, as through some of my endless nights, I realised that for me, there's nothing more exciting and fulfilling than research!

I can't exclude the Erasmus mobility office; whose generous financial contribution is the reason as to why this opportunity was made achievable in the first place.

Finally, I extend special thanks to the almighty God, who has graced me with all the good that I see in my life, and my family who have been readily available for support, either emotional, financial, among others. I've had the opportunity to interface with several amazing people in Madrid. We can only wait to see what the future holds but being granted an opportunity to meet them once more would be a great pleasure.

APPENDIX

MATLAB code implemented for the nano spheres:

Initialization of variables for the planar array of nanospheres

```
N = 500;   % Number of elements used in the lattice sum
M = N;
H = 500;   % Number of plane waves used in the lattice sum

AB = 300e-9;      % Reference lattice constant
a = AB;           % Lattice constant in the "x" axis
b = AB;    % Lattice constant in the "y" axis

K1 = linspace(0.1,1,500)*2*pi/a;
lamb = 2*pi./K1; % Wavelength
Ang1 = linspace(0,89.5,180)*pi/180;       % Angle of incidence, with respect
to the "z" axis

K2 = linspace(0.1,1,10000)*2*pi/a;
lamb_int = 2*pi./K2;     % Wavelength after interpolation
Ang_int = linspace(0,89.5,3600)*pi/180;

th = pi/2;       % Lattice definition ("th = pi/2" rectangular lattice, "th
= pi/3" and "a = b" triangular lattice)
alpha2 = 0*pi/180;      % Incident angle respect to the lattice plane ("xy"
plane)

eps = 1;         % 2.1025
mu = 1;
nk = sqrt(eps.*mu);     % Refractive index of the external medium

X = 0;           % Array with the positions of the particles in the unit
cell
Y = 0;

mainFolder = '/Users/kabonire/Desktop/CEMD_Code';
functionsFolder = '/Users/kabonire/Desktop/CEMD_Code/Functions';
mieCoefficientsFolder=
'/Users/kabonire/Desktop/CEMD_Code/Functions/MieCoefficientFunctions';
imagesFolder = '/Users/kabonire/Desktop/CEMD_Code/Images';
dataFolder = '/Users/kabonire/Desktop/CEMD_Code/R and T';
```

To compute the depolarization Green function

```
% If it is already calculated, go to the next module
% Gga = GbCalc_NUC(a,b,th,N,M,H,X,Y,lamb,Ang1,alpha2,nk);

cd(mainFolder);
load('Gga.mat')
```

Interpolation of the Green function

```
 cd(functionsFolder);
 Gga_int = interp_Gga_1pUC_kx(lamb,Ang1,Gga,lamb_int,Ang_int);
```

Sphere polarizability calculated with the Mie theory

```
  cd(mieCoefficientsFolder);
 K = 2.*pi./lamb_int*nk;             % External medium wavevector

 R = a/4;                 % Sphere Radius
 eps1 = 3.5.^2;          % Sphere Permitivity
 mu1 = 1;          % Sphere Permeability (the polarizability expressions used
in this code only work from mu1 = mu = 1);

 nk1 = sqrt(eps1.*mu1)./nk;

 x = K.*R;         % Size parameter

 a1 = (nk1*shi(1,nk1*x).*dshi(1,x) -
shi(1,x).*dshi(1,nk1*x))./(nk1*shi(1,nk1*x).*dchi(1,x) -
 chi(1,x).*dshi(1,nk1*x));     % a1 Mie coefficient

 b1 = (shi(1,nk1.*x).*dshi(1,x) -
nk1*shi(1,x).*dshi(1,nk1*x))./(shi(1,nk1*x).*dchi(1,x) -
 nk1*chi(1,x).*dshi(1,nk1*x));       % b1 Mie coefficient

 ae = 1i.*6.*pi./K.*a1;   % Electric polarizability
 am = 1i.*6.*pi./K.*b1;  % Magnetic polarizability

 % Calculating the diffraction order
 % ("n = m = 0" for the specular mode)
 n = 0;
 m = 0;

 for l=1:length(lamb_int)

      k = 2.*pi./(lamb_int(l)).*nk;

      for j = 1:length(Ang_int)

            ang1 = Ang_int(j);

 % The polarizability matrix is built from the polarizability values;

 alpe1 = ae(l)*eye(3); % Electric polarizability of the particle,
 alpm1 = am(l)*eye(3); % Magnetic polarizability of the particle
 alp1 = [alpe1,zeros(3,3);zeros(3,3),alpm1]; % Polarizability of the particle
(6*6 matrix)

 Gg = GsN(l,j,Gga_int,X,Y); % Building the depolarization Green function

 [ErTM,EtTM,ErTE,EtTE] = Ert_2Dg_NUC(a,b,X,Y,ang1,alpha2,k,n,m,alp1,Gg,th);
```

```
% The incident electric field for TE and TM polarisation
EiTM = [cos(ang1).*cos(alpha2),cos(ang1).*sin(alpha2),-sin(ang1),-
sin(alpha2),cos(alpha2),0]';
EiTE = [sin(alpha2),-
cos(alpha2),0,cos(ang1).*cos(alpha2),cos(ang1).*sin(alpha2),-sin(ang1)]';

% Reflectance (Reflectivity) and Transmittance (Transmissivity)
     rtm = abs(ErTM./EiTM).^2;
     rte = abs(ErTE./EiTE).^2;
     ttm = abs(EtTM./EiTM).^2;
     tte = abs(EtTE./EiTE).^2;

     TTEa(l,j) = tte(4);
     RTEa(l,j) = rte(4);
     TTMa(l,j) = ttm(1);
     RTMa(l,j) = rtm(1);

     TTEb(l,j) = tte(2);
     RTEb(l,j) = rte(2);
     TTMb(l,j) = ttm(5);
     RTMb(l,j) = rtm(5);

% Reflection and Transmission coefficient

     rcte = ErTE./EiTE;
     tcte = EtTE./EiTE;
     rctm = ErTM./EiTM;
     tctm = EtTM./EiTM;

     RcaTE(l,j) = rcte(4); % Hx=4(a), Ey=2(b)
     TcaTE(l,j) = tcte(4);
     RcbTE(l,j) = rcte(2);
     TcbTE(l,j) = tcte(2);

     RcaTM(l,j) = rctm(1); % Ex=1(a), Hy=5(b)
     TcaTM(l,j) = tctm(1);
     RcbTM(l,j) = rctm(5);
     TcbTM(l,j) = tctm(5);

% Used with the Stokes plots (normalisation of the field components)

     exer = (ErTE(2)./-1);
     exet = (EtTE(2)./-1);
     hxmr = (ErTM(5).*-1);
     hxmt = (EtTM(5));

     RTMxa(l,j) = hxmr;
     RTExa(l,j) = exer;
     TTMxa(l,j) = hxmt;
     TTExa(l,j) = exet;
     end
end

cd(imagesFolder);

close all
```

Reflectance plots for TE and TM

```
figure
[LL,AA] = meshgrid(lamb_int,Ang_int*180/pi);
surf(1./LL*a,AA,real(TTEa'),'edgecolor' , 'none');view(2); shading interp;
colorbar;
title('Transmittance with TE polarization Re (Hx)','FontSize',
14,'Interpreter','tex'),
ylabel('\theta (deg)','FontSize',12),
xlabel('ka/2\pi','FontSize',12),
set(gca,'LooseInset',get(gca,'TightInset'));
set(gca,'XLim',[0.3 0.85])
set(gca,'YLim',[0 89.5])
saveas(gcf,'TTEaRe.tif')

figure
[LL,AA] = meshgrid(lamb_int,Ang_int*180/pi);
surf(1./LL*a,AA,real(RTEa'),'edgecolor' , 'none');view(2); shading interp;
colorbar;
title('Reflectance with TE polarization Re (Hx)','FontSize',
14,'Interpreter','tex'),
ylabel('\theta (deg)','FontSize',12),
xlabel('ka/2\pi','FontSize',12),
set(gca,'LooseInset',get(gca,'TightInset'));
set(gca,'XLim',[0.3 0.85])
set(gca,'YLim',[0 89.5])
saveas(gcf,'RTEaRe.tif')

figure
[LL,AA] = meshgrid(lamb_int,Ang_int*180/pi);
surf(1./LL*a,AA,real(TTMa'),'edgecolor' , 'none');view(2); shading interp;
colorbar;
title('Transmittance with TM polarization Re (Ex)','FontSize',
14,'Interpreter','tex'),
ylabel('\theta (deg)','FontSize',12),
xlabel('ka/2\pi','FontSize',12),
set(gca,'LooseInset',get(gca,'TightInset'));
set(gca,'XLim',[0.3 0.85])
set(gca,'YLim',[0 89.5])
saveas(gcf,'TTMaRe.tif')

figure
[LL,AA] = meshgrid(lamb_int,Ang_int*180/pi);
surf(1./LL*a,AA,real(RTMa'),'edgecolor' , 'none');view(2); shading interp;
colorbar;
title('Reflectance with TM polarization Re (Ex)','FontSize',
14,'Interpreter','tex'),
ylabel('\theta (deg)','FontSize',12),
xlabel('ka/2\pi','FontSize',12),
set(gca,'LooseInset',get(gca,'TightInset'));
set(gca,'XLim',[0.3 0.85])
set(gca,'YLim',[0 89.5])
saveas(gcf,'RTMaRe.tif')
```

Reflection and Transmission coefficients

```
% real
figure
[LL,AA] = meshgrid(lamb_int,Ang_int*180/pi);
surf(1./LL*a,AA,real(RcaTE'),'edgecolor' , 'none');view(2); shading interp;
colorbar; caxis([-1 1]);
title('Reflection coefficient with TE polarization Re (Hx)','FontSize',
14,'Interpreter','tex'),
ylabel('\theta (deg)','FontSize',12),
xlabel('ka/2\pi','FontSize',12),
set(gca,'LooseInset',get(gca,'TightInset'));
set(gca,'XLim',[0.3 0.85])
set(gca,'YLim',[0 89.5])
saveas(gcf,'RcaTERe.tif')

figure
[LL,AA] = meshgrid(lamb_int,Ang_int*180/pi);
surf(1./LL*a,AA,real(TcaTE'),'edgecolor' , 'none');view(2); shading interp;
colorbar; caxis([-1 1]);
title('Transmission coefficeint with TE polarization Re (Hx)','FontSize',
14,'Interpreter','tex'),
ylabel('\theta (deg)','FontSize',12),
xlabel('ka/2\pi','FontSize',12),
set(gca,'LooseInset',get(gca,'TightInset'));
set(gca,'XLim',[0.3 0.85])
set(gca,'YLim',[0 89.5])
saveas(gcf,'TcaTERe.tif')

figure
[LL,AA] = meshgrid(lamb_int,Ang_int*180/pi);
surf(1./LL*a,AA,real(RcbTE'),'edgecolor' , 'none');view(2); shading interp;
colorbar; caxis([-1 1]);
surf(1./LL*a,AA,real((RcbTE./-1)'),'edgecolor' , 'none');view(2); shading
interp; colorbar; caxis([-1 1]);
title('Reflection coefficient with TE polarization Re (Ey)','FontSize',
14,'Interpreter','tex'),
ylabel('\theta (deg)','FontSize',12),
xlabel('ka/2\pi','FontSize',12),
set(gca,'LooseInset',get(gca,'TightInset'));
set(gca,'XLim',[0.3 0.85])
set(gca,'YLim',[0 89.5])
saveas(gcf,'RcbTERe.tif')

figure
[LL,AA] = meshgrid(lamb_int,Ang_int*180/pi);
surf(1./LL*a,AA,real(TcbTE'),'edgecolor' , 'none');view(2); shading interp;
colorbar; caxis([-1 1]);
surf(1./LL*a,AA,real((TcbTE./-1)'),'edgecolor' , 'none');view(2); shading
interp; colorbar; caxis([-1 1]);
title('Transmission coefficient with TE polarization Re (Ey)','FontSize',
14,'Interpreter','tex'),
ylabel('\theta (deg)','FontSize',12),
xlabel('ka/2\pi','FontSize',12),
set(gca,'LooseInset',get(gca,'TightInset'));
set(gca,'XLim',[0.3 0.85])
```

```
set(gca,'YLim',[0 89.5])
saveas(gcf,'TcbTERe.tif')

figure
[LL,AA] = meshgrid(lamb_int,Ang_int*180/pi);
surf(1./LL*a,AA,real(RcaTM'),'edgecolor' , 'none');view(2); shading interp;
colorbar; caxis([-1 1]);
title('Reflection coefficient with TM polarization Re (Ex)','FontSize',
14,'Interpreter','tex'),
ylabel('\theta (deg)','FontSize',12),
xlabel('ka/2\pi','FontSize',12),
set(gca,'LooseInset',get(gca,'TightInset'));
set(gca,'XLim',[0.3 0.85])
set(gca,'YLim',[0 89.5])
saveas(gcf,'RcaTMRe.tif')

figure
[LL,AA] = meshgrid(lamb_int,Ang_int*180/pi);
surf(1./LL*a,AA,real(TcaTM'),'edgecolor' , 'none');view(2); shading interp;
colorbar; caxis([-1 1]);
title('Transmission coefficient with TM polarization Re (Ex)','FontSize',
14,'Interpreter','tex'),
ylabel('\theta (deg)','FontSize',12),
xlabel('ka/2\pi','FontSize',12),
set(gca,'LooseInset',get(gca,'TightInset'));
set(gca,'XLim',[0.3 0.85])
set(gca,'YLim',[0 89.5])
saveas(gcf,'TcaTMRe.tif')

figure
[LL,AA] = meshgrid(lamb_int,Ang_int*180/pi);
surf(1./LL*a,AA,real(RcbTM'),'edgecolor' , 'none');view(2); shading interp;
colorbar; caxis([-1 1]);
surf(1./LL*a,AA,real((RcbTM.*-1)'),'edgecolor' , 'none');view(2); shading
interp; colorbar; caxis([-1 1]);
title('Reflection coefficient with TM polarization Re (Hy)','FontSize',
14,'Interpreter','tex'),
ylabel('\theta (deg)','FontSize',12),
xlabel('ka/2\pi','FontSize',12),
set(gca,'LooseInset',get(gca,'TightInset'));
set(gca,'XLim',[0.3 0.85])
set(gca,'YLim',[0 89.5])
saveas(gcf,'RcbTMRe.tif')

figure
[LL,AA] = meshgrid(lamb_int,Ang_int*180/pi);
surf(1./LL*a,AA,real(TcbTM'),'edgecolor' , 'none');view(2); shading interp;
colorbar; caxis([-1 1]);
title('Transmission coefficient with TM polarization Re (Hy)','FontSize',
14,'Interpreter','tex'),
ylabel('\theta (deg)','FontSize',12),
xlabel('ka/2\pi','FontSize',12),
set(gca,'LooseInset',get(gca,'TightInset'));
set(gca,'XLim',[0.3 0.85])
set(gca,'YLim',[0 89.5])
saveas(gcf,'TcbTMRe.tif')
```

Stokes I, Q, U and V parameters for the generated polarisations

```
% Polarisation in reflection

% +45° Linear polarisation in reflection

lte = 1/sqrt(2);
ltm = 1/sqrt(2);
RTEx = lte.*RTExa;
RTMx = ltm.*RTMxa;

I = abs(RTEx).^2 + abs(RTMx).^2;
Qa = abs(RTEx).^2 - abs(RTMx).^2;
Ua = 2.*real(RTEx.*conj(RTMx));
Va = 2.*imag(RTEx.*conj(RTMx));
Q = Qa./I;
U = Ua./I;
V = Va./I;

figure
[LL,AA] = meshgrid(lamb_int,Ang_int*180/pi);
surf(1./LL*a,AA,real(I'),'edgecolor' , 'none'); view(2); shading interp;
colorbar; caxis([-1 1]);
title({'I Stokes parameter for +45°'; 'linear polarisation in
reflection'},'FontSize', 14,'Interpreter','tex'),
ylabel('\theta (deg)','FontSize',12),
xlabel('ka/2\pi','FontSize',12),
set(gca,'LooseInset',get(gca,'TightInset'));
set(gca, 'Xlim', [0.3 0.85])
set(gca, 'Ylim', [0 89.5])
saveas(gcf,'I Stokes +45 polarisation in reflection.tif')

figure
[LL,AA] = meshgrid(lamb_int,Ang_int*180/pi);
surf(1./LL*a,AA,real(Q'),'edgecolor' , 'none'); view(2); shading interp;
colorbar; caxis([-1 1]);
title({'Q Stokes parameter for +45°'; 'linear polarisation in
reflection'},'FontSize', 14,'Interpreter','tex'),
ylabel('\theta (deg)','FontSize',12),
xlabel('ka/2\pi','FontSize',12),
set(gca,'LooseInset',get(gca,'TightInset'));
set(gca, 'Xlim', [0.3 0.85])
set(gca, 'Ylim', [0 89.5])
saveas(gcf,'Q Stokes +45 polarisation in reflection.tif')

figure
[LL,AA] = meshgrid(lamb_int,Ang_int*180/pi);
surf(1./LL*a,AA,real(U'),'edgecolor' , 'none'); view(2); shading interp;
colorbar; caxis([-1 1]);
title({'U Stokes parameter for +45°'; 'linear polarisation in
reflection'},'FontSize', 14,'Interpreter','tex'),
ylabel('\theta (deg)','FontSize',12),
xlabel('ka/2\pi','FontSize',12),
set(gca,'LooseInset',get(gca,'TightInset'));
set(gca, 'Xlim', [0.3 0.85])
set(gca, 'Ylim', [0 89.5])
```

```
saveas(gcf,'U Stokes +45 polarisation in reflection.tif')

figure
[LL,AA] = meshgrid(lamb_int,Ang_int*180/pi);
surf(1./LL*a,AA,real(V'),'edgecolor' , 'none'); view(2); shading interp;
colorbar; caxis([-1 1]);
title({'V Stokes parameter for +45°'; 'linear polarisation in
reflection'},'FontSize', 14,'Interpreter','tex'),
ylabel('\theta (deg)','FontSize',12),
xlabel('ka/2\pi','FontSize',12),
set(gca,'LooseInset',get(gca,'TightInset'));
set(gca, 'Xlim', [0.3 0.85])
set(gca, 'Ylim', [0 89.5])
saveas(gcf,'V Stokes +45 polarisation in reflection.tif')

% -45° Linear polarisation in reflection

lte = 1/sqrt(2);
ltm = -1/sqrt(2);
RTEx = lte.*RTExa;
RTMx = ltm.*RTMxa;

I = abs(RTEx).^2 + abs(RTMx).^2;
Qa = abs(RTEx).^2 - abs(RTMx).^2;
Ua = 2.*real(RTEx.*conj(RTMx));
Va = 2.*imag(RTEx.*conj(RTMx));
Q = Qa./I;
U = Ua./I;
V = Va./I;

figure
[LL,AA] = meshgrid(lamb_int,Ang_int*180/pi);
surf(1./LL*a,AA,real(I'),'edgecolor' , 'none'); view(2); shading interp;
colorbar; caxis([-1 1]);
title({'I Stokes parameter for -45°'; 'linear polarisation in
reflection'},'FontSize', 14,'Interpreter','tex'),
ylabel('\theta (deg)','FontSize',12),
xlabel('ka/2\pi','FontSize',12),
set(gca,'LooseInset',get(gca,'TightInset'));
set(gca, 'Xlim', [0.3 0.85])
set(gca, 'Ylim', [0 89.5])
saveas(gcf,'I Stokes -45 polarisation in reflection.tif')

figure
[LL,AA] = meshgrid(lamb_int,Ang_int*180/pi);
surf(1./LL*a,AA,real(Q'),'edgecolor' , 'none'); view(2); shading interp;
colorbar; caxis([-1 1]);
title({'Q Stokes parameter for -45°'; 'linear polarisation in
reflection'},'FontSize', 14,'Interpreter','tex'),
ylabel('\theta (deg)','FontSize',12),
xlabel('ka/2\pi','FontSize',12),
set(gca,'LooseInset',get(gca,'TightInset'));
set(gca, 'Xlim', [0.3 0.85])
set(gca, 'Ylim', [0 89.5])
saveas(gcf,'Q Stokes -45 polarisation in reflection.tif')
```

```
figure
[LL,AA] = meshgrid(lamb_int,Ang_int*180/pi);
surf(1./LL*a,AA,real(U'),'edgecolor' , 'none'); view(2); shading interp;
colorbar; caxis([-1 1]);
title({'U Stokes parameter for -45°'; 'linear polarisation in
reflection'},'FontSize', 14,'Interpreter','tex'),
ylabel('\theta (deg)','FontSize',12),
xlabel('ka/2\pi','FontSize',12),
set(gca,'LooseInset',get(gca,'TightInset'));
set(gca, 'Xlim', [0.3 0.85])
set(gca, 'Ylim', [0 89.5])
saveas(gcf,'U Stokes -45 polarisation in reflection.tif')

figure
[LL,AA] = meshgrid(lamb_int,Ang_int*180/pi);
surf(1./LL*a,AA,real(V'),'edgecolor' , 'none'); view(2); shading interp;
colorbar; caxis([-1 1]);
title({'V Stokes parameter for -45°'; 'linear polarisation in
reflection'},'FontSize', 14,'Interpreter','tex'),
ylabel('\theta (deg)','FontSize',12),
xlabel('ka/2\pi','FontSize',12),
set(gca,'LooseInset',get(gca,'TightInset'));
set(gca, 'Xlim', [0.3 0.85])
set(gca, 'Ylim', [0 89.5])
saveas(gcf,'V Stokes -45 polarisation in reflection.tif')

% TE Linear polarisation in reflection

lte = 1;
ltm = 0;
RTEx = lte.*RTExa;
RTMx = ltm.*RTMxa;
I = abs(RTEx).^2 + abs(RTMx).^2;

figure
[LL,AA] = meshgrid(lamb_int,Ang_int*180/pi);
surf(1./LL*a,AA,real(I'),'edgecolor' , 'none'); view(2); shading interp;
colorbar; caxis([-1 1]);
title('I Stokes parameter for TE polarisation in reflection','FontSize',
14,'Interpreter','tex'),
ylabel('\theta (deg)','FontSize',12),
xlabel('ka/2\pi','FontSize',12),
set(gca,'LooseInset',get(gca,'TightInset'));
set(gca, 'Xlim', [0.3 0.85])
set(gca, 'Ylim', [0 89.5])
saveas(gcf,'I Stokes TE polarisation in reflection.tif')

% TM Linear polarisation in reflection

lte = 0;
ltm = 1;
RTEx = lte.*RTExa;
RTMx = ltm.*RTMxa;

I = abs(RTEx).^2 + abs(RTMx).^2;
```

```
figure
[LL,AA] = meshgrid(lamb_int,Ang_int*180/pi);
surf(1./LL*a,AA,real(I'),'edgecolor' , 'none'); view(2); shading interp;
colorbar; caxis([-1 1]);
title('I Stokes parameter for TM polarisation in reflection','FontSize',
14,'Interpreter','tex'),
ylabel('\theta (deg)','FontSize',12),
xlabel('ka/2\pi','FontSize',12),
set(gca,'LooseInset',get(gca,'TightInset'));
set(gca, 'Xlim', [0.3 0.85])
set(gca, 'Ylim', [0 89.5])
saveas(gcf,'I Stokes TM polarisation in reflection.tif')

% Right-handed circular polarisation in reflection

cte = 1/sqrt(2);
ctm = 1i/sqrt(2);
RTEx = cte.*RTExa;
RTMx = ctm.*RTMxa;

I = abs(RTEx).^2 + abs(RTMx).^2;
Qa = abs(RTEx).^2 - abs(RTMx).^2;
Ua = 2.*real(RTEx.*conj(RTMx));
Va = 2.*imag(RTEx.*conj(RTMx));
Q = Qa./I;
U = Ua./I;
V = Va./I;

figure
[LL,AA] = meshgrid(lamb_int,Ang_int*180/pi);
surf(1./LL*a,AA,real(I'),'edgecolor' , 'none'); view(2); shading interp;
colorbar; caxis([-1 1]);
title({'I Stokes parameter for right-handed'; 'circular polarisation in
reflection'},'FontSize', 14,'Interpreter','tex'),
ylabel('\theta (deg)','FontSize',12),
xlabel('ka/2\pi','FontSize',12),
set(gca,'LooseInset',get(gca,'TightInset'));
set(gca, 'Xlim', [0.3 0.85])
set(gca, 'Ylim', [0 89.5])
saveas(gcf,'I Stokes rgt cir polarisation in reflection.tif')

figure
[LL,AA] = meshgrid(lamb_int,Ang_int*180/pi);
surf(1./LL*a,AA,real(Q'),'edgecolor' , 'none'); view(2); shading interp;
colorbar; caxis([-1 1]);
title({'Q Stokes parameter for right-handed'; 'circular polarisation in
reflection'},'FontSize', 14,'Interpreter','tex'),
ylabel('\theta (deg)','FontSize',12),
xlabel('ka/2\pi','FontSize',12),
set(gca,'LooseInset',get(gca,'TightInset'));
set(gca, 'Xlim', [0.3 0.85])
set(gca, 'Ylim', [0 89.5])
saveas(gcf,'Q Stokes rgt cir polarisation in reflection.tif')
```

```
figure
[LL,AA] = meshgrid(lamb_int,Ang_int*180/pi);
surf(1./LL*a,AA,real(U'),'edgecolor' , 'none'); view(2); shading interp;
colorbar; caxis([-1 1]);
title({'U Stokes parameter for right-handed'; 'circular polarisation in
reflection'},'FontSize', 14,'Interpreter','tex'),
ylabel('\theta (deg)','FontSize',12),
xlabel('ka/2\pi','FontSize',12),
set(gca,'LooseInset',get(gca,'TightInset'));
set(gca, 'Xlim', [0.3 0.85])
set(gca, 'Ylim', [0 89.5])
saveas(gcf,'U Stokes rgt cir polarisation in reflection.tif')

figure
[LL,AA] = meshgrid(lamb_int,Ang_int*180/pi);
surf(1./LL*a,AA,real(V'),'edgecolor' , 'none'); view(2); shading interp;
colorbar; caxis([-1 1]);
title({'V Stokes parameter for right-handed'; 'circular polarisation in
reflection'},'FontSize', 14,'Interpreter','tex'),
ylabel('\theta (deg)','FontSize',12),
xlabel('ka/2\pi','FontSize',12),
set(gca,'LooseInset',get(gca,'TightInset'));
set(gca, 'Xlim', [0.3 0.85])
set(gca, 'Ylim', [0 89.5])
saveas(gcf,'V Stokes rgt cir polarisation in reflection.tif')

% Left-handed circular polarisation in reflection

cte = 1/sqrt(2);
ctm = -1i/sqrt(2);
RTEx = cte.*RTExa;
RTMx = ctm.*RTMxa;

I = abs(RTEx).^2 + abs(RTMx).^2;
Qa = abs(RTEx).^2 - abs(RTMx).^2;
Ua = 2.*real(RTEx.*conj(RTMx));
Va = 2.*imag(RTEx.*conj(RTMx));
Q = Qa./I;
U = Ua./I;
V = Va./I;

figure
[LL,AA] = meshgrid(lamb_int,Ang_int*180/pi);
surf(1./LL*a,AA,real(I'),'edgecolor' , 'none'); view(2); shading interp;
colorbar; caxis([-1 1]);
title({'I Stokes parameter for left-handed'; 'circular polarisation in
reflection'},'FontSize', 14,'Interpreter','tex'),
ylabel('\theta (deg)','FontSize',12),
xlabel('ka/2\pi','FontSize',12),
set(gca,'LooseInset',get(gca,'TightInset'));
set(gca, 'Xlim', [0.3 0.85])
set(gca, 'Ylim', [0 89.5])
saveas(gcf,'I Stokes lft cir polarisation in reflection.tif')
```

```
figure
[LL,AA] = meshgrid(lamb_int,Ang_int*180/pi);
surf(1./LL*a,AA,real(I'),'edgecolor' , 'none'); view(2); shading interp;
colorbar; caxis([-1 1]);
title({'I Stokes parameter for left-handed'; 'circular polarisation in
reflection'},'FontSize', 14,'Interpreter','tex'),
ylabel('\theta (deg)','FontSize',12),
xlabel('ka/2\pi','FontSize',12),
set(gca,'LooseInset',get(gca,'TightInset'));
set(gca, 'Xlim', [0.5 0.8])
set(gca, 'Ylim', [0 40])
saveas(gcf,'I Stokes zoom lft cir polarisation in reflection.tif')

figure
[LL,AA] = meshgrid(lamb_int,Ang_int*180/pi);
surf(1./LL*a,AA,real(Q'),'edgecolor' , 'none'); view(2); shading interp;
colorbar; caxis([-1 1]);
title({'Q Stokes parameter for left-handed'; 'circular polarisation in
reflection'},'FontSize', 14,'Interpreter','tex'),
ylabel('\theta (deg)','FontSize',12),
xlabel('ka/2\pi','FontSize',12),
set(gca,'LooseInset',get(gca,'TightInset'));
set(gca, 'Xlim', [0.3 0.85])
set(gca, 'Ylim', [0 89.5])
saveas(gcf,'Q Stokes lft cir polarisation in reflection.tif')

figure
[LL,AA] = meshgrid(lamb_int,Ang_int*180/pi);
surf(1./LL*a,AA,real(U'),'edgecolor' , 'none'); view(2); shading interp;
colorbar; caxis([-1 1]);
title({'U Stokes parameter for left-handed'; 'circular polarisation in
reflection'},'FontSize', 14,'Interpreter','tex'),
ylabel('\theta (deg)','FontSize',12),
xlabel('ka/2\pi','FontSize',12),
set(gca,'LooseInset',get(gca,'TightInset'));
set(gca, 'Xlim', [0.3 0.85])
set(gca, 'Ylim', [0 89.5])
saveas(gcf,'U Stokes lft cir polarisation in reflection.tif')

figure
[LL,AA] = meshgrid(lamb_int,Ang_int*180/pi);
surf(1./LL*a,AA,real(V'),'edgecolor' , 'none'); view(2); shading interp;
colorbar; caxis([-1 1]);
title({'V Stokes parameter for left-handed'; 'circular polarisation in
reflection'},'FontSize', 14,'Interpreter','tex'),
ylabel('\theta (deg)','FontSize',12),
xlabel('ka/2\pi','FontSize',12),
set(gca,'LooseInset',get(gca,'TightInset'));
set(gca, 'Xlim', [0.3 0.85])
set(gca, 'Ylim', [0 89.5])
saveas(gcf,'V Stokes lft cir polarisation in reflection.tif')
```

```
figure
[LL,AA] = meshgrid(lamb_int,Ang_int*180/pi);
surf(1./LL*a,AA,real(V'),'edgecolor' , 'none'); view(2); shading interp;
colorbar; caxis([-1 1]);
title({'V Stokes parameter for left-handed'; 'circular polarisation in
reflection'},'FontSize', 14,'Interpreter','tex'),
ylabel('\theta (deg)','FontSize',12),
xlabel('ka/2\pi','FontSize',12),
set(gca,'LooseInset',get(gca,'TightInset'));
set(gca, 'Xlim', [0.5 0.8])
set(gca, 'Ylim', [0 40])
saveas(gcf,'V Stokes zoom lft cir polarisation in reflection.tif')

% Polarisation in transmission

% 45° Linear polarisation in transmission

lte = 1/sqrt(2);
ltm = 1/sqrt(2);
TTEx = lte.*TTExa;
TTMx = ltm.*TTMxa;

I = abs(TTEx).^2 + abs(TTMx).^2;
Qa = abs(TTEx).^2 - abs(TTMx).^2;
Ua = real(2.*(TTEx.*conj(TTMx)));
Va = imag(2.*(TTEx.*conj(TTMx)));
Q = Qa./I;
U = Ua./I;
V = Va./I;

figure
[LL,AA] = meshgrid(lamb_int,Ang_int*180/pi);
surf(1./LL*a,AA,real(I'),'edgecolor' , 'none'); view(2); shading interp;
colorbar; caxis([-1 1]);
title({'I Stokes parameter for +45°'; 'linear polarisation in
transmission'},'FontSize', 14,'Interpreter','tex'),
ylabel('\theta (deg)','FontSize',12),
xlabel('ka/2\pi','FontSize',12),
set(gca,'LooseInset',get(gca,'TightInset'));
set(gca, 'Xlim', [0.3 0.85])
set(gca, 'Ylim', [0 89.5])
saveas(gcf,'I Stokes +45 polarisation in transmission.tif')

figure
[LL,AA] = meshgrid(lamb_int,Ang_int*180/pi);
surf(1./LL*a,AA,real(Q'),'edgecolor' , 'none'); view(2); shading interp;
colorbar; caxis([-1 1]);
title({'Q Stokes parameter for +45°'; 'linear polarisation in
transmission'},'FontSize', 14,'Interpreter','tex'),
ylabel('\theta (deg)','FontSize',12),
xlabel('ka/2\pi','FontSize',12),
set(gca,'LooseInset',get(gca,'TightInset'));
set(gca, 'Xlim', [0.3 0.85])
set(gca, 'Ylim', [0 89.5])
saveas(gcf,'Q Stokes +45 polarisation in transmission.tif')
```

```
figure
[LL,AA] = meshgrid(lamb_int,Ang_int*180/pi);
surf(1./LL*a,AA,real(U'),'edgecolor' , 'none'); view(2); shading interp;
colorbar; caxis([-1 1]);
title({'U Stokes parameter for +45°'; 'linear polarisation in
transmission'},'FontSize', 14,'Interpreter','tex'),
ylabel('\theta (deg)','FontSize',12),
xlabel('ka/2\pi','FontSize',12),
set(gca,'LooseInset',get(gca,'TightInset'));
set(gca, 'Xlim', [0.3 0.85])
set(gca, 'Ylim', [0 89.5])
saveas(gcf,'U Stokes +45 polarisation in transmission.tif')

figure
[LL,AA] = meshgrid(lamb_int,Ang_int*180/pi);
surf(1./LL*a,AA,real(V'),'edgecolor' , 'none'); view(2); shading interp;
colorbar; caxis([-1 1]);
title({'V Stokes parameter for +45°'; 'linear polarisation in
transmission'},'FontSize', 14,'Interpreter','tex'),
ylabel('\theta (deg)','FontSize',12),
xlabel('ka/2\pi','FontSize',12),
set(gca,'LooseInset',get(gca,'TightInset'));
set(gca, 'Xlim', [0.3 0.85])
set(gca, 'Ylim', [0 89.5])
saveas(gcf,'V Stokes +45 polarisation in transmission.tif')

% -45° Linear polarisation in transmission

lte = 1/sqrt(2);
ltm = -1/sqrt(2);
TTEx = lte.*TTExa;
TTMx = ltm.*TTMxa;

I = abs(TTEx).^2 + abs(TTMx).^2;
Qa = abs(TTEx).^2 - abs(TTMx).^2;
Ua = real(2.*(TTEx.*conj(TTMx)));
Va = imag(2.*(TTEx.*conj(TTMx)));
Q = Qa./I;
U = Ua./I;
V = Va./I;

figure
[LL,AA] = meshgrid(lamb_int,Ang_int*180/pi);
surf(1./LL*a,AA,real(I'),'edgecolor' , 'none'); view(2); shading interp;
colorbar; caxis([-1 1]);
title({'I Stokes parameter for -45°'; 'linear polarisation in
transmission'},'FontSize', 14,'Interpreter','tex'),
ylabel('\theta (deg)','FontSize',12),
xlabel('ka/2\pi','FontSize',12),
set(gca,'LooseInset',get(gca,'TightInset'));
set(gca, 'Xlim', [0.3 0.85])
set(gca, 'Ylim', [0 89.5])
saveas(gcf,'I Stokes -45 polarisation in transmission.tif')
```

```
figure
[LL,AA] = meshgrid(lamb_int,Ang_int*180/pi);
surf(1./LL*a,AA,real(Q'),'edgecolor' , 'none'); view(2); shading interp;
colorbar; caxis([-1 1]);
title({'Q Stokes parameter for -45°'; 'linear polarisation in
transmission'},'FontSize', 14,'Interpreter','tex'),
ylabel('\theta (deg)','FontSize',12),
xlabel('ka/2\pi','FontSize',12),
set(gca,'LooseInset',get(gca,'TightInset'));
set(gca, 'Xlim', [0.3 0.85])
set(gca, 'Ylim', [0 89.5])
saveas(gcf,'Q Stokes -45 polarisation in transmission.tif')

figure
[LL,AA] = meshgrid(lamb_int,Ang_int*180/pi);
surf(1./LL*a,AA,real(U'),'edgecolor' , 'none'); view(2); shading interp;
colorbar; caxis([-1 1]);
title({'U Stokes parameter for -45°'; 'linear polarisation in
transmission'},'FontSize', 14,'Interpreter','tex'),
ylabel('\theta (deg)','FontSize',12),
xlabel('ka/2\pi','FontSize',12),
set(gca,'LooseInset',get(gca,'TightInset'));
set(gca, 'Xlim', [0.3 0.85])
set(gca, 'Ylim', [0 89.5])
saveas(gcf,'U Stokes -45 polarisation in transmission.tif')

figure
[LL,AA] = meshgrid(lamb_int,Ang_int*180/pi);
surf(1./LL*a,AA,real(V'),'edgecolor' , 'none'); view(2); shading interp;
colorbar; caxis([-1 1]);
title({'V Stokes parameter for -45°'; 'linear polarisation in
transmission'},'FontSize', 14,'Interpreter','tex'),
ylabel('\theta (deg)','FontSize',12),
xlabel('ka/2\pi','FontSize',12),
set(gca,'LooseInset',get(gca,'TightInset'));
set(gca, 'Xlim', [0.3 0.85])
set(gca, 'Ylim', [0 89.5])
saveas(gcf,'V Stokes -45 polarisation in transmission.tif')

% TE Linear polarisation in transmission

lte = 1;
ltm = 0;
TTEx = lte.*TTExa;
TTMx = ltm.*TTMxa;

I = abs(TTEx).^2 + abs(TTMx).^2;

figure
[LL,AA] = meshgrid(lamb_int,Ang_int*180/pi);
surf(1./LL*a,AA,real(I'),'edgecolor' , 'none'); view(2); shading interp;
colorbar; caxis([-1 1]);
title('I Stokes parameter for TE polarisation in transmission','FontSize',
14,'Interpreter','tex'),
ylabel('\theta (deg)','FontSize',12),
```

```
xlabel('ka/2\pi','FontSize',12),
set(gca,'LooseInset',get(gca,'TightInset'));
set(gca, 'Xlim', [0.3 0.85])
set(gca, 'Ylim', [0 89.5])
saveas(gcf,'I Stokes TE polarisation in transmission.tif')

% TM Linear polarisation in transmission

lte = 0;
ltm = 1;
TTEx = lte.*TTExa;
TTMx = ltm.*TTMxa;

I = abs(TTEx).^2 + abs(TTMx).^2;

figure
[LL,AA] = meshgrid(lamb_int,Ang_int*180/pi);
surf(1./LL*a,AA,real(I'),'edgecolor' , 'none'); view(2); shading interp;
colorbar; caxis([-1 1]);
title('I Stokes parameter for TM polarisation in transmission','FontSize',
14,'Interpreter','tex'),
ylabel('\theta (deg)','FontSize',12),
xlabel('ka/2\pi','FontSize',12),
set(gca,'LooseInset',get(gca,'TightInset'));
set(gca, 'Xlim', [0.3 0.85])
set(gca, 'Ylim', [0 89.5])
saveas(gcf,'I Stokes TM polarisation in transmission.tif')

% Right-handed circular polarisation in transmission

cte = 1/sqrt(2);
ctm = 1i/sqrt(2);
TTEx = cte.*TTExa;
TTMx = ctm.*TTMxa;

I = abs(TTEx).^2 + abs(TTMx).^2;
Qa = abs(TTEx).^2 - abs(TTMx).^2;
Ua = real(2.*(TTEx.*conj(TTMx)));
Va = imag(2.*(TTEx.*conj(TTMx)));
Q = Qa./I;
U = Ua./I;
V = Va./I;

figure
[LL,AA] = meshgrid(lamb_int,Ang_int*180/pi);
surf(1./LL*a,AA,real(I'),'edgecolor' , 'none'); view(2); shading interp;
colorbar; caxis([-1 1]);
title({'I Stokes parameter for right-handed'; 'circular polarisation in
transmission'},'FontSize', 14,'Interpreter','tex'),
ylabel('\theta (deg)','FontSize',12),
xlabel('ka/2\pi','FontSize',12),
set(gca,'LooseInset',get(gca,'TightInset'));
set(gca, 'Xlim', [0.3 0.85])
set(gca, 'Ylim', [0 89.5])
saveas(gcf,'I Stokes rgt cir polarisation in transmission.tif')
```

```
figure
[LL,AA] = meshgrid(lamb_int,Ang_int*180/pi);
surf(1./LL*a,AA,real(Q'),'edgecolor' , 'none'); view(2); shading interp;
colorbar; caxis([-1 1]);
title({'Q Stokes parameter for right-handed'; 'circular polarisation in
transmission'},'FontSize', 14,'Interpreter','tex'),
ylabel('\theta (deg)','FontSize',12),
xlabel('ka/2\pi','FontSize',12),
set(gca,'LooseInset',get(gca,'TightInset'));
set(gca, 'Xlim', [0.3 0.85])
set(gca, 'Ylim', [0 89.5])
saveas(gcf,'Q Stokes rgt cir polarisation in transmission.tif')

figure
[LL,AA] = meshgrid(lamb_int,Ang_int*180/pi);
surf(1./LL*a,AA,real(U'),'edgecolor' , 'none'); view(2); shading interp;
colorbar; caxis([-1 1]);
title({'U Stokes parameter for right-handed'; 'circular polarisation in
transmission'},'FontSize', 14,'Interpreter','tex'),
ylabel('\theta (deg)','FontSize',12),
xlabel('ka/2\pi','FontSize',12),
set(gca,'LooseInset',get(gca,'TightInset'));
set(gca, 'Xlim', [0.3 0.85])
set(gca, 'Ylim', [0 89.5])
saveas(gcf,'U Stokes rgt cir polarisation in transmission.tif')

figure
[LL,AA] = meshgrid(lamb_int,Ang_int*180/pi);
surf(1./LL*a,AA,real(V'),'edgecolor' , 'none'); view(2); shading interp;
colorbar; caxis([-1 1]);
title({'V Stokes parameter for right-handed'; 'circular polarisation in
transmission'},'FontSize', 14,'Interpreter','tex'),
ylabel('\theta (deg)','FontSize',12),
xlabel('ka/2\pi','FontSize',12),
set(gca,'LooseInset',get(gca,'TightInset'));
set(gca, 'Xlim', [0.3 0.85])
set(gca, 'Ylim', [0 89.5])
saveas(gcf,'V Stokes rgt cir polarisation in transmission.tif')

% Left-handed circular polarisation in transmission

cte = 1/sqrt(2);
ctm = -1i/sqrt(2);
TTEx = cte.*TTExa;
TTMx = ctm.*TTMxa;

I = abs(TTEx).^2 + abs(TTMx).^2;
Qa = abs(TTEx).^2 - abs(TTMx).^2;
Ua = real(2.*(TTEx.*conj(TTMx)));
Va = imag(2.*(TTEx.*conj(TTMx)));
Q = Qa./I;
U = Ua./I;
V = Va./I;
```

```
figure
[LL,AA] = meshgrid(lamb_int,Ang_int*180/pi);
surf(1./LL*a,AA,real(I'),'edgecolor' , 'none'); view(2); shading interp;
colorbar; caxis([-1 1]);
title({'I Stokes parameter for left-handed'; 'circular polarisation in
transmission'},'FontSize', 14,'Interpreter','tex'),
ylabel('\theta (deg)','FontSize',12),
xlabel('ka/2\pi','FontSize',12),
set(gca,'LooseInset',get(gca,'TightInset'));
set(gca, 'Xlim', [0.3 0.85])
set(gca, 'Ylim', [0 89.5])
saveas(gcf,'I Stokes lft cir polarisation in transmission.tif')

figure
[LL,AA] = meshgrid(lamb_int,Ang_int*180/pi);
surf(1./LL*a,AA,real(I'),'edgecolor' , 'none'); view(2); shading interp;
colorbar; caxis([-1 1]);
title({'I Stokes parameter for left-handed'; 'circular polarisation in
transmission'},'FontSize', 14,'Interpreter','tex'),
ylabel('\theta (deg)','FontSize',12),
xlabel('ka/2\pi','FontSize',12)
set(gca,'LooseInset',get(gca,'TightInset'));
set(gca, 'Xlim', [0.53 0.78])
set(gca, 'Ylim', [0 40])
saveas(gcf,'I Stokes zoom lft cir polarisation in transmission.tif')

figure
[LL,AA] = meshgrid(lamb_int,Ang_int*180/pi);
surf(1./LL*a,AA,real(Q'),'edgecolor' , 'none'); view(2); shading interp;
colorbar; caxis([-1 1]);
title({'Q Stokes parameter for left-handed'; 'circular polarisation in
transmission'},'FontSize', 14,'Interpreter','tex'),
ylabel('\theta (deg)','FontSize',12),
xlabel('ka/2\pi','FontSize',12),
set(gca,'LooseInset',get(gca,'TightInset'));
set(gca, 'Xlim', [0.3 0.85])
set(gca, 'Ylim', [0 89.5])
saveas(gcf,'Q Stokes lft cir polarisation in transmission.tif')

figure
[LL,AA] = meshgrid(lamb_int,Ang_int*180/pi);
surf(1./LL*a,AA,real(U'),'edgecolor' , 'none'); view(2); shading interp;
colorbar; caxis([-1 1]);
title({'U Stokes parameter for left-handed'; 'circular polarisation in
transmission'},'FontSize', 14,'Interpreter','tex'),
ylabel('\theta (deg)','FontSize',12),
xlabel('ka/2\pi','FontSize',12),
set(gca,'LooseInset',get(gca,'TightInset'));
set(gca, 'Xlim', [0.3 0.85])
set(gca, 'Ylim', [0 89.5])
saveas(gcf,'U Stokes lft cir polarisation in transmission.tif')

figure
[LL,AA] = meshgrid(lamb_int,Ang_int*180/pi);
surf(1./LL*a,AA,real(V'),'edgecolor' , 'none'); view(2); shading interp;
```

```
colorbar; caxis([-1 1]);
title({'V Stokes parameter for left-handed'; 'circular polarisation in
transmission'},'FontSize', 14,'Interpreter','tex'),
ylabel('\theta (deg)','FontSize',12),
xlabel('ka/2\pi','FontSize',12),
set(gca,'LooseInset',get(gca,'TightInset'));
set(gca, 'Xlim', [0.3 0.85])
set(gca, 'Ylim', [0 89.5])
saveas(gcf,'V Stokes lft cir polarisation in transmission.tif')

figure
[LL,AA] = meshgrid(lamb_int,Ang_int*180/pi);
surf(1./LL*a,AA,real(V'),'edgecolor' , 'none'); view(2); shading interp;
colorbar; caxis([-1 1]);
title({'V Stokes parameter for left-handed'; 'circular polarisation in
transmission'},'FontSize', 14,'Interpreter','tex'),
ylabel('\theta (deg)','FontSize',12),
xlabel('ka/2\pi','FontSize',12),
set(gca,'LooseInset',get(gca,'TightInset'));
set(gca, 'Xlim', [0.53 0.78])
set(gca, 'Ylim', [0 40])
saveas(gcf,'V Stokes zoom lft cir polarisation in transmission.tif')
```

Identified BIC regions

```
% Lower-frequency BIC
```

Left-handed circular polarisation in transmission

```
cte = 1/sqrt(2);
ctm = -1i/sqrt(2);
TTEx = cte.*TTExa;
TTMx = ctm.*TTMxa;

I = abs(TTEx).^2 + abs(TTMx).^2;
Va = imag(2.*(TTEx.*conj(TTMx)));
V = Va./I;

figure
[LL,AA] = meshgrid(lamb_int,Ang_int*180/pi);
surf(1./LL*a,AA,real(V'),'edgecolor' , 'none'); view(2); shading interp;
colorbar; caxis([-1 1]);
title({'V Stokes parameter for normalised left-handed'; 'circular
polarisation in transmission'},'FontSize', 14,'Interpreter','tex'),
ylabel('\theta (deg)','FontSize',12),
xlabel('ka/2\pi','FontSize',12),
set(gca,'LooseInset',get(gca,'TightInset'));
set(gca, 'Xlim', [0.562 0.567])
set(gca, 'Ylim', [0 10])
saveas(gcf,'V Stokes nLCT BIC1.tif')

figure
[LL,AA] = meshgrid(lamb_int,Ang_int*180/pi);
surf(1./LL*a,AA,real(Va'),'edgecolor' , 'none'); view(2); shading interp;
colorbar; caxis([-1 1]);
title({'V Stokes parameter for left-handed'; 'circular polarisation in
```

```
transmission'},'FontSize', 14,'Interpreter','tex'),
ylabel('\theta (deg)','FontSize',12),
xlabel('ka/2\pi','FontSize',12),
set(gca,'LooseInset',get(gca,'TightInset'));
set(gca, 'Xlim', [0.562 0.567])
set(gca, 'Ylim', [0 10])
saveas(gcf,'V Stokes LCT BIC1.tif')
```

```
% Higher-frequency BIC
```

Left-handed circular polarisation in transmission

```
cte = 1/sqrt(2);
ctm = -1i/sqrt(2);
TTEx = cte.*TTExa;
TTMx = ctm.*TTMxa;

I = abs(TTEx).^2 + abs(TTMx).^2;
Va = imag(2.*(TTEx.*conj(TTMx)));
V = Va./I;

figure
[LL,AA] = meshgrid(lamb_int,Ang_int*180/pi);
surf(1./LL*a,AA,real(V'),'edgecolor' , 'none'); view(2); shading interp;
colorbar; caxis([-1 1]);
title({'V Stokes parameter for normalised left-handed'; 'circular
polarisation in transmission'},'FontSize', 14,'Interpreter','tex'),
ylabel('\theta (deg)','FontSize',12),
xlabel('ka/2\pi','FontSize',12),
set(gca,'LooseInset',get(gca,'TightInset'));
set(gca, 'Xlim', [0.736 0.740])
set(gca, 'Ylim', [0 10])
saveas(gcf,'V Stokes nLCT BIC2.tif')

figure
[LL,AA] = meshgrid(lamb_int,Ang_int*180/pi);
surf(1./LL*a,AA,real(Va'),'edgecolor' , 'none'); view(2); shading interp;
colorbar; caxis([-1 1]);
title({'V Stokes parameter for left-handed'; 'circular polarisation in
transmission'},'FontSize', 14,'Interpreter','tex'),
ylabel('\theta (deg)','FontSize',12),
xlabel('ka/2\pi','FontSize',12),
set(gca,'LooseInset',get(gca,'TightInset'));
set(gca, 'Xlim', [0.736 0.740])
set(gca, 'Ylim', [0 10])
saveas(gcf,'V Stokes LCT BIC2.tif')
```

BIC Transmittance values isolated at different angles

```
k = (2*pi)./lamb_int;
freq = (k.*a)./(2*pi);

cte_t = 1/sqrt(2);
ctmr_t = 1i/sqrt(2);
ctml_t = -1i/sqrt(2);
TTEx_c = cte_t.*TTExa;
TTMxr_c = ctmr_t.*TTMxa;
TTMxl_c = ctml_t.*TTMxa;
I_rgt_t = abs(TTEx_c).^2 + abs(TTMxr_c).^2;
I_lft_t = abs(TTEx_c).^2 + abs(TTMxl_c).^2;
V_rt = 2.*imag(TTEx_c.*conj(TTMxr_c));
V_lft = 2.*imag(TTEx_c.*conj(TTMxl_c));
V_rgt_t = V_rt./I_rgt_t;
V_lft_t = V_lt./I_lft_t;

figure
plot(freq,real(V_lft_t(:,402)),'b','LineWidth',1.1)
hold on
plot(freq,real(V_lft_t(:,321)),'g','LineWidth',1.1)
plot(freq,real(V_lft_t(:,241)),'r','LineWidth',1.1)
plot(freq,real(V_lft_t(:,201)),'c','LineWidth',1.1)
plot(freq,real(V_lft_t(:,150)),'m','LineWidth',1.1)
plot(freq,real(V_lft_t(:,100)),'y','LineWidth',1.1)
plot(freq,real(V_lft_t(:,60)),'k','LineWidth',1.1)
plot(freq,real(I_lft_t(:,402)),'b-.','LineWidth',1.1)
plot(freq,real(I_lft_t(:,321)),'g-.','LineWidth',1.1)
plot(freq,real(I_lft_t(:,241)),'r-.','LineWidth',1.1)
plot(freq,real(I_lft_t(:,201)),'c-.','LineWidth',1.1)
plot(freq,real(I_lft_t(:,150)),'m-.','LineWidth',1.1)
plot(freq,real(I_lft_t(:,100)),'y-.','LineWidth',1.1)
plot(freq,real(I_lft_t(:,60)),'k-.','LineWidth',1.1)
hold off;
ylabel('Transmittance','FontSize',12),
xlabel('ka/2\pi','FontSize',12),
set(gca,'LooseInset',get(gca,'TightInset'));
set(gca,'XLim',[0.3 0.85])
title({'I and V Stokes parameters at varying angles of
incidence';'(Lefthanded
circular polarisation)'},'FontSize', 14,'Interpreter','tex'),
grid; legend('V 9.99694°','V 7.98263°','V 5.99319°','V 4.99847°','V
3.73020°','V 2.48680°','V 1.49208°','I 9.99694°','I 7.98263°','I
5.99319°','I
4.99847°','I 3.73020°','I 2.48680°','I 1.49208°');
set(legend,'units','pixels');
set(legend,'location','BestOutside','FontSize',10);
saveas(gcf,'Entire spectrum.tif')

figure
plot(freq,real(V_lft_t(:,402)),'b','LineWidth',1.1)
hold on
plot(freq,real(V_lft_t(:,321)),'g','LineWidth',1.1)
plot(freq,real(V_lft_t(:,241)),'r','LineWidth',1.1)
plot(freq,real(V_lft_t(:,201)),'c','LineWidth',1.1)
```

```
 plot(freq,real(V_lft_t(:,150)),'m','LineWidth',1.1)
 plot(freq,real(V_lft_t(:,100)),'y','LineWidth',1.1)
 plot(freq,real(V_lft_t(:,60)),'k','LineWidth',1.1)
 plot(freq,real(I_lft_t(:,402)),'b-.','LineWidth',1.1)
 plot(freq,real(I_lft_t(:,321)),'g-.','LineWidth',1.1)
 plot(freq,real(I_lft_t(:,241)),'r-.','LineWidth',1.1)
 plot(freq,real(I_lft_t(:,201)),'c-.','LineWidth',1.1)
 plot(freq,real(I_lft_t(:,150)),'m-.','LineWidth',1.1)
 plot(freq,real(I_lft_t(:,100)),'y-.','LineWidth',1.1)
 plot(freq,real(I_lft_t(:,60)),'k-.','LineWidth',1.1)
 hold off;
 ylabel('Transmittance','FontSize',12),
 xlabel('ka/2\pi','FontSize',12),
 set(gca,'LooseInset',get(gca,'TightInset'));
 set(gca,'XLim',[0.563 0.565])
 title({'I and V Stokes parameters at varying angles of incidence';'for BIC 1
 (Left-handed circular polarisation)'},'FontSize', 14,'Interpreter','tex'),
 grid; legend('V 9.99694°','V 7.98263°','V 5.99319°','V 4.99847°','V
 3.73020°','V 2.48680°','V 1.49208°','I 9.99694°','I 7.98263°','I
5.99319°','I
 4.99847°','I 3.73020°','I 2.48680°','I 1.49208°');
 set(legend,'units','pixels');
 set(legend,'location','BestOutside','FontSize',10);
 saveas(gcf,'BIC1_lct.tif')

 figure
 plot(freq,real(V_lft_t(:,402)),'b','LineWidth',1.1)
 hold on
 plot(freq,real(V_lft_t(:,321)),'g','LineWidth',1.1)
 plot(freq,real(V_lft_t(:,241)),'r','LineWidth',1.1)
 plot(freq,real(V_lft_t(:,201)),'c','LineWidth',1.1)
 plot(freq,real(V_lft_t(:,150)),'m','LineWidth',1.1)
 plot(freq,real(V_lft_t(:,100)),'y','LineWidth',1.1)
 plot(freq,real(V_lft_t(:,60)),'k','LineWidth',1.1)
 plot(freq,real(I_lft_t(:,402)),'b-.','LineWidth',1.1)
 plot(freq,real(I_lft_t(:,321)),'g-.','LineWidth',1.1)
 plot(freq,real(I_lft_t(:,241)),'r-.','LineWidth',1.1)
 plot(freq,real(I_lft_t(:,201)),'c-.','LineWidth',1.1)
 plot(freq,real(I_lft_t(:,150)),'m-.','LineWidth',1.1)
 plot(freq,real(I_lft_t(:,100)),'y-.','LineWidth',1.1)
 plot(freq,real(I_lft_t(:,60)),'k-.','LineWidth',1.1)
 hold off;
 ylabel('Transmittance','FontSize',12),
 xlabel('ka/2\pi','FontSize',12),
 set(gca,'LooseInset',get(gca,'TightInset'));
 set(gca,'XLim',[0.736 0.740])
 title({'I and V Stokes parameters at varying angles of incidence';'for BIC 2
 (Left-handed circular polarisation)'},'FontSize', 14,'Interpreter','tex'),
 grid; legend('V 9.99694°','V 7.98263°','V 5.99319°','V 4.99847°','V
 3.73020°','V 2.48680°','V 1.49208°','I 9.99694°','I 7.98263°','I
5.99319°','I
 4.99847°','I 3.73020°','I 2.48680°','I 1.49208°');
 set(legend,'units','pixels');
 set(legend,'location','BestOutside','FontSize',10);
 saveas(gcf,'BIC2_lct.tif')
```

To note:

```
% Details of the polarizability:
% Considering particles defined by diagonal polarizabilities, The
polarizabilities of the particle at [X, Y] are;
% Aex = Electric polarizability component "xx"
% Aey = Electric polarizability component "yy"
% Aez = Electric polarizability component "zz"
% Amx = Magnetic polarizability component "xx"
% Amy = Magnetic polarizability component "yy"
% Amz = Magnetic polarizability component "zz"
% Polarizability units the polarizability are [m].
% Considering the Mie theory, the polarizability of a dielectric sphere is
given as;
% electric polarizability (ae) = 1i.*6.*pi./k.*a1;
% magnetic polarizability (am) = 1i.*6.*pi./k.*b1;
% where "a1" and "b1" are the addimensional Mie coefficients.
```